Experimental and numerical study on behaviour of square steel tube confined reinforced concrete stub columns after fire exposure

Liu, Faqi; Yang, Hua; Yan, Rui; Wang, Wei

DOI
10.1016/j.tws.2019.02.037

Publication date
2019

Document Version
Accepted author manuscript

Published in
Thin-Walled Structures

Experimental and numerical study on behaviour of square steel tube confined reinforced concrete stub columns after fire exposure

Faqi Liu [a,b], Hua Yang [a,b], Rui Yan[c], Wei Wang[a,b]

[a] Key Lab of Structures Dynamic Behavior and Control of the Ministry of Education, Harbin Institute of Technology, Harbin, 150090, China

[b] Key Lab of Smart Prevention and Mitigation of Civil Engineering Disasters of the Ministry of Industry and Information Technology, Harbin Institute of Technology, Harbin, 150090, China

[c] Delft University of Technology, Faculty of Civil Engineering and Geosciences, Stevinweg 1, 2600 GA Delft, The Netherlands

Abstract:

The behaviour of square steel tube confined reinforced concrete columns after fire exposure was studied experimentally and numerically in this paper. Eighteen stub columns were first heated following the ISO 834 standard fire including both heating and cooling phases, and were subsequently loaded to failure after cooling to ambient temperature. Failure modes, temperatures in specimens, axial load versus deformation curves and strains in steel tube were monitored and discussed. A finite element model was developed using the sequentially coupled thermal-stress analysis method and was validated against tests found in literatures and this study . Parametric study was performed to identify influences of key parameters, where are heating time, cross-sectional dimension, strengths of materials, steel tube to concrete area ratio and reinforcement ratio, on residual capacity and compressive stiffness. Finally, a simplified method is proposed for predicting residual cross-sectional capacity and compressive stiffness of square steel tube confined reinforced concrete columns after fire exposure.

Key words: square steel tube confined reinforced concrete; compressive stiffness; post-fire; residual capacity; test; numerical simulation

Nomenclature

A_b	cross-sectional area of reinforcing bars
A_c	cross-sectional area of concrete core
A_s	cross-sectional area of steel tube
B	width of square section
d_b	diameter of bars
EA	compressive stiffness of column
E_b	Young's modulus of reinforcement at ambient temperature
E_{bT}	Young's modulus of reinforcement after fire exposure
E_c	Young's modulus of concrete at ambient temperature
E_{cT}	Young's modulus of concrete after fire exposure
E_s	Young's modulus of steel at ambient temperature
E_{sT}	Young's modulus of steel after fire exposure
f_b	yield strength of reinforcement at ambient temperature
f_{bu}	ultimate tensile strength of reinforcement
f_{bT}	yield strength of reinforcement after fire exposure
f_{ck}	characteristic concrete strength, f_{ck}=0.67 f_{cu}
f_{cu}	concrete cube strength
$f_{cu,28}$	concrete cube strength at 28 days
$f_{cu,test}$	concrete cube strength at the test day of the specimens
f_c'	concrete cylinder strength
f_{cT}'	concrete cylinder strength after fire exposure
f_{tT}'	concrete tensile strength after fire exposure
f_{su}	ultimate tensile strength of structural steel
f_y	yield strength of steel at ambient temperature
f_{yT}	yield strength of steel after fire exposure
k	factor accounting for the delay of temperature rise of concrete
L	length of column
N_y	yield load of composite column

N_u	ultimate capacity of composite column
t_h	heating time to the maximum fire temperature
t_s	wall thickness of the steel tube
T	temperature
T_{max}	the maximum temperature achieved during the heating and cooling phases
α_b	ratio of reinforcement, $\alpha_b=A_b/A_c$
α_s	steel tube to concrete area ratio, $\alpha_s=A_s/A_c$
ε_{bf}	percentage elongation at fracture of reinforcement
ε_{sf}	percentage elongation at fracture of structural steel
$\mu_\triangle$	ductility index
v_s	Poisson's ratio of structural steel
ξ	confinement factor, $\xi= f_y A_s/f_{ck} A_c$
σ_v	longitudinal stress in steel tube
σ_h	transverse stress in steel tube
σ_z	equivalent stress in steel tube, $\sigma_z=\frac{\sqrt{2}}{2}\sqrt{(\sigma_v-\sigma_h)^2+\sigma_v^2+\sigma_h^2}$
$\triangle_y$	displacement at yield load
$\triangle_u$	displacement at ultimate load
$\triangle_{0.85}$	displacement at $0.85N_u$ after peak load

1. Introduction

Steel tube confined reinforced concrete (STCRC) column is a kind of composite member possessing high load-bearing performance and excellent seismic resistance. It resembles concrete-filled steel tubular (CFST) column in appearance. Differs to CFST column, a key feature of the STCRC column is the discontinuity of the steel tube at beam to column joints. It is therefore that the steel tube is pressure free from the longitudinal force and applies a considerable radial constraint to the concrete which consequently increases the strength as well as the ductility of the concrete. Local buckling of steel tube also can be delayed or avoided which enables the application of thin-walled steel tube in STCRC columns. If the same amount of steel is used in the STCRC column as that in CFST column, most of steel could be used to bear axial load and bending moment in the form of reinforcing bars embedded in concrete sustain c for the STCRC column, and thus a better fire performance than the CFST column can be expected. The STCRC column to reinforced concrete (RC) beam joints resemble that in reinforced concrete structures, which avoids the complexity of CFST column to RC beam joints. Typical square STCRC columns in practice are shown in Fig.1 [1].

In order to prevent brittle shear failure and improve deformability of reinforced concrete stub columns, Tomii et al. [2, 3] first proposed the STCRC column in 1985. To date, extensive researches have been carried out on the static and seismic performance of this kind of column. Sakino et al. [4], Han et al. [5], Liu and Zhou [6], Yu et al. [7], Gan [8], Liu et al. [9, 10], Zhou et al. [11] and Wang and Liu [1] studied the behaviours of circular or square STCRC stub columns or slender columns under axial or eccentric compression. It was found that lateral confining stress provided by the steel tube greatly enhances the load-bearing capacity and ductility of this kind of member. Aboutaha et al. [12], Han et al. [13], Zhou and Liu [14] and Liu et al. [15] investigated seismic resistance of rectangular, circular or square STCRC columns or STCRC column to RC beam joints. These studies reveal that ductility of STCRC columns decreases with increase of axial load ratio. However, they exhibit higher flexural capacity, higher ductility and greater ability to dissipate energy than RC columns, especially when subjected to high compressive load levels. The authors investigated the behaviours of circular STCRC columns after fire exposure, including cross-section behaviour [16], buckling bebaviour [17] and behaivour under combined compression and bending [18]. It was found that heating time and cross-sectional dimension have significant influence on load-bearing capacity and compressive stiffness. Although some crushing occurred in concrete, the concrete remained largely intact due to the confinement of the outer steel tube [17], which prevented falling off of the concrete cover and then reinforcing bars were maintained at low temperatures. Strength of steel recovers partially after cooling to room temperature while the strength of concrete after exposure is unrecoverable, thus confinement effect enhances relatively and more ductile behaviour is observed after fire exposure. STCRC columns after fire exposure have good residual perfromance and possibility of rehabilitation. Square shaped steel tube confined reinforced concrete columns are already applied in engineering practice in China, such as the project shown in Fig.1. Different to circular STCRC columns, the square section provides non-uniform confinement to concrete, which results in different performance from circular columns. However, no study related on post-fire behaviour of this kind of column is available. Therefore the subject of this paper focuses on the post-fire behaviour of square STCRC columns.

Eighteen square STCRC stub columns were heated following the ISO 834 standard fire curve including both heating and cooling phases. After cooling to room temperatures, these columns were axially loaded to failure. Temperatures in fire furnace and in specimens, axial load-deformation curves and strains of steel tube were recorded. Failure modes were observed and discussed. The sequentially coupled thermal-stress analysis method was adopted to develop a finite element model, which was validated against this test and related tests in literatures. Influences of key parameters on the residual capacity and compressive stiffness of the square STCRC column were studied, including heating time, cross-sectional dimension, steel tube to concrete area ratio, reinforcement ratio and strengths of materials. Finally, a simplified design method was recommended for evaluating the cross-section capacity and compressive stiffness of square STCRC columns after fire exposure.

2. Experimental investigation

2.1 Specimens

The investigation includes an experimental study on 18 square steel tube confined reinforced concrete (STCRC) columns. Variables in the test include heating time (t_h=0min, 45min, 90min) and cross-section dimension (B=200mm and 250mm, where B is the width of the square section). The steel tube to concrete area ratio α_s ($\alpha_s = A_s/A_c$, where A_s and A_c are the cross-section area of steel tube and concrete, respectively) was 3.70% and 3.62% respectively for specimen with a section width of 200 mm and 250 mm. The reinforcement ratio α_b ($\alpha_b = A_b/A_c$, where A_b is the cross-section area of reinforcing bars) was 4.17%. Lengths of specimens were three times widths of cross section, to ensure the stub column behaviour and avoid the end effect. Specifications of the specimens are outlined in Table 1. A general view and layout of reinforcing bars are shown in Fig.2.

Steel sheets were cold-formed into U sections and then seam welded to square sections, as shown in Fig.2. Hot-rolled ribbed bars are used for the longitudinal reinforcing bars and hot-rolled plain bars are used as stirrups. Eight longitudinal reinforcing bars were tied with 8 mm stirrups at 200 mm intervals. The concrete cover from external surface of the concrete to outer perimeter of the longitudinal reinforcing bars was 25 mm. The end plates welded to these columns were 10 mm thick. Two strips with a width of 10 mm were cut from the outer steel tube after casting concrete, 50 mm away from each end, to simulate the break of steel tube at beam to column joints in practice. Then two gaps were introduced, which can be used as vent holes for releasing water vapor during heating process. Details of the specimens are illustrated in Fig.2.

In order to measure cross-section temperatures during the heating process, four additional specimens were specially fabricated. According to cross-section dimensions and heating time, these specimens are referred as S200-45min, S200-90min, S250-45min and S250-90min, respectively. The steel tube, reinforcing bars, stirrups and concrete of these four columns were the same as other corresponding specimens. Temperatures across the section of these specimens were measured with 1 mm K type thermocouples. Layouts of thermocouples are shown in Fig.3.

2.2 Material properties

Table 2 presents tensile coupon test results of steel tube before and after fire exposure, which were tested according to ISO 6892-1 [19]. In Table 2, E_s is elastic modulus, f_y is yield strength, f_{su} is ultimate strength, ν_s is Poisson's ratio and ε_{sf} is percentage elongation at fracture. Fire exposure results in decrease of both elastic modulus and strength. Fig.4 presents measured stress-strain relationship curves. These curves are close to the idealised elastic-perfectly plastic stress-strain relationship up to 3.0% strain for both the unexposed and exposed condition, which is far more than the strain of steel tube during testing. Hence the idealised elastic-perfectly plastic stress-strain relationship model was employed in finite element analysis. The properties of reinforcing bars obtained from tensile coupon test are given in Table 3, where d_b is the diameter, E_b is the elastic modulus, f_b is the yield strength, f_{bu} is the ultimate tensile strength and ε_{sf} is the percentage elongation at fracture.

Ready-mixed concrete was used to cast the specimens in this study. 150 mm × 150 mm × 150 mm concrete cubes and 150 mm × 150 mm × 300 mm concrete prisms were casted with the same batch of concrete as these specimens to measure the concrete cube strength and elastic modulus, respectively. The measured compressive strength and elastic modulus are given in Table 4, in which $f_{cu,28}$ is the cube strength after curing for 28 days, $f_{cu,test}$ and $E_{c,test}$ are the cube strength and elastic modulus on the day of testing specimens, respectively, v_c is the Poisson's ratio of concrete.

2.3 Test setup and procedure

The square STCRC columns were unloaded during heating process since it is a more conservative condition for evaluating residual strength of concrete [20-22] and concrete members [23] after fire exposure. The heating test was conducted in a furnace built at Harbin Institute of Technology, which can be used for testing columns, beams and slabs under combined structural and fire loading. Details of the furnace are described in [16]. The ISO 834 standard fire curve including both heating and cooling phases [24] was employed in the test. To prevent heat from being transferred into specimens via end plates, ceramic fibre blankets were attached to both ends of these specimens. Furnace temperatures and temperatures of steel tube, reinforcing bars and concrete were measured during the heating process.

After cooing to room temperature, these square STCRC columns were tested using a 5000 kN hydraulic compression machine. A load cell and four linear variable displacement transducers (LVDTs) were used to measure the axial load level and axial displacement, respectively. To ensure a uniform compression was applied on these columns, data of these LVDTs were monitored at the early stages of loading. Strain gauges were placed on the outer surface of steel tube in longitudinal direction and transverse direction, at the mid-height and at the edge of the top break of steel tube, to measure the longitudinal and transverse strains. Axial load, axial deformation and strains of steel tube were measured during the loading process.

2.4 Test results and discussions

Typical failure modes of these specimens and the failure modes of inner concrete are presented in Fig.6. The unexposed specimens and the exposed specimens with heating time of 45 min were failed by shear failure, which means confinement of outer steel tube cannot fully prevent shear failure of the inner concrete in these columns. However, outward buckling of steel tube and concrete crushing were observed in specimens with heating time of 90 min, indicating a more ductile behavior. Deterioration of concrete strength caused by high temperature is irreversible, whereas partial strength of steel recovers after cooling to room temperature, therefore the corresponding confinement effect enhances relatively after fire exposure.

The measured furnace temperatures agree well with the ISO 834 standard fire curve during the whole heating process (including heating and cooling phases) [24], as shown in Fig.7, which proved the accuracy of the fire furnace. Furnace temperature was controlled to decrease at a rate of 10.417 ^{o}C /min to 200 ^{o}C during the cooling phase, after which no cooling curve is specified in the ISO 834 standard [24]. The measured cooling rate was pretty low after cooling down lower than 200 ^{o}C, which can be attributed to the heat emitted from the insulation materials of the furnace and specimens.

The measured temperatures of steel tube, reinforcing bars and concrete at different locations along the height and cross-section are presented in Fig.8. The temperatures of corresponding thermocouples at different heights, e.g., 1 and 6, 5 and 10, 2 and 7, 3 and 8, 4 and 9, confirming temperature uniformities along the specimen length.

The peak temperatures decrease from the outer surface to the concrete centre, whereas the corresponding time increases significantly. Take the specimen S200-45min for example, the peak temperatures and corresponding time of steel tube, reinforcing bar and concrete centre are 757 ^{o}C 45min, 392 ^{o}C 80 min and 338 ^{o}C 150 min, respectively. This can be explained by the high thermal capacity of the concrete. Due to 2-D heat transfer at the cross-section corner, temperatures of the reinforcing bars at corner are higher than those of other reinforcing bars, as shown in Fig.8. Temperatures of some points are missing in Fig.8 since these thermocouples broken in the preparation of specimens, including thermocouple 7, 8, 11, 14 of specimen S200-90 min and thermocouple 3, 4, 14 of specimen S250-90 min.

Axial load - displacement curves are illustrated in Fig.9. The axial load - displacement curve is almost linear till 0.8 times of the peak load, followed by a decreased stiffness to the peak load, after that the load decreases gradually. The compressive stiffness EA, the yield load N_{y} and the peak load N_{u}, the displacement at the yield load $\triangle_{\mathrm{y}}$, the displacement at the peak load $\triangle_{\mathrm{u}}$, the displacement at $0.85N_{\mathrm{u}}$ after the peak load $\triangle_{0.85}$ and the ductility index $\mu_{\triangle}$ ($\mu_{\triangle}=\triangle_{0.85}/\triangle_{\mathrm{y}}$) are given in Table 5. The yield load and corresponding displacement were determined according to the method described in [16].

The influences of heating time on the load-bearing capacity, compressive stiffness and ductility index of square STCRC columns are shown in Fig.10. Both the load-bearing capacity and compressive stiffness decrease with the increase of heating time, whereas the ductility index increases correspondingly. The reduction of load-bearing capacity reaches 17.59% and 47.28% for specimens with heating time of 45 min and 90 min respectively relative to that of the unexposed specimens, whereas the corresponding stiffness of these specimens decreases by 38.95% and 55.68%, respectively. It reveals that the deterioration of compressive stiffness is more severe than the load-bearing capacity, which consists with test results of concrete material after exposure to high temperatures [25]. The ductility index increases by 12.04% and 30.56% for specimens with heating time of 45 min and 90 min respectively relative to that of the unexposed specimens, which can be explained by the enhancement of confinement effect after exposure. Since steel strength was recovered partially after cooling to room temperature while the degradation of concrete was irreversible after exposure, therefore confinement effect of steel tube to concrete increases relatively.

The measured longitudinal and transverse strains of steel tube during loading process were used to capture the development of stresses. The elastic-perfectly plastic stress-strain relationship model was employed for the steel tube. Typical axial load versus steel stress curves for unexposed and exposed specimens are shown in Fig.11, in which σ_{h} is the transverse stress, σ_{v} is the longitudinal stress, and σ_{z} is the equivalent stress ($\sigma_{\mathrm{z}}=\frac{\sqrt{2}}{2}\sqrt{(\sigma_{\mathrm{v}}-\sigma_{\mathrm{h}})^2+\sigma_{\mathrm{v}}^2+\sigma_{\mathrm{h}}^2}$). As shown in Fig.11 (a) and (b), the longitudinal stresses are close to the transverse stresses in steel tube for unexposed specimen. The reason is that the bond and friction between steel tube and concrete transferred axial load to the steel tube, which is different from the pure confine condition as expected. The longitudinal stresses of steel tube in specimens after fire exposure are much lower than corresponding transverse stresses (Fig.11 (c) to (f)), which means the steel tube in these specimens is more effective to provide confinement effect to concrete. This phenomenon may be explained by the reduction of the bond strength between the steel tube and concrete after fire exposure [26].

3. Finite element analysis

The sequentially coupled thermal-stress analysis method was employed to develop a finite element (FE) model using program ABAQUS to further study behaviours of square STCRC columns after fire exposure. Firstly pure heat transfer analysis was performed to obtain thermal profiles and then temperature results were read into a stress analysis.

3.1 Heat transfer analysis

Steel tube, concrete and reinforcing bars were modeled using 4-node quadrilateral shell heat transfer elements (DS4), 8-node linear brick heat transfer elements (DC3D8) and 2-node link heat transfer elements (DC1D2), respectively. Thermal properties of steel and concrete were defined using models proposed by Lie [27], which has been successfully applied by the authors for simulation of circular STCRC columns [16-18]. The influence of moisture evaporation was taken into consideration by modifying the specific heat of concrete and the content of water was taken as 5% by weight.

Heat is transferred from fire to outer surface of columns via convection and radiation, and then finally to columns by conduction. The ISO 834 standard fire curve [24] was defined as thermal load, which includes both heating and cooling phases. A convective coefficient of 25W/(m^2K) and a resultant emissivity of 0.5 were employed in this study. Thermal resistance at the interface between steel tube and concrete was taken as 0.01 (m^2K)/W [28-30].

3.2 Stress analysis

In order to import temperature results efficiently and correctly, meshes of the stress analysis model remained the same as those of thermal analysis model. However, elements were changed to be stress analysis elements. Steel tube, concrete and reinforcing bars were modeled using 4-node shell elements with reduced integration (S4R), 8-node linear brick elements with reduced integration

(C3D8R) and 2-node linear truss elements (T3D2), respectively.

The interfacial behaviour between steel tube and concrete was simulated using the surface to surface contact, with Coulomb friction model in the tangential direction and hard contact in the normal direction. The friction coefficient was taken as 0.3. The bond strength at the interfacial surface was taken as 0.15 MPa for the square STCRC columns, regardless of exposed or unexposed columns [26]. Reinforcing bars were embedded in the concrete.

The corner zone of the cold-formed steel section possesses higher yield strength than the flat zone due to the strain hardening behaviour [31]. Since the square hollow sections used in STCRC columns had pretty large width to thickness ratios, the area ratios of the corner zone to the whole section were relative small which approximately turn out to be 3%. Finite element analysis results showed that the strain hardening behaviour has negligible influence on the bearing capacity of square STCRC columns. Therefore the strain hardening effect of corner zone was not considered in latter analysis.

The elastic-perfectly plastic stress-strain relationship model was employed for structural steel and reinforcing bars. The residual elastic modulus of structural steel and reinforcing bars after fire exposure can be calculated as [32]:

$$E_{sT} = \begin{cases} E_s & T_{max} \leq 500^{o}C \\ [1-1.30\times10^{-4}(T_{max}-500)]E_s & T_{max} > 500^{o}C \end{cases} \tag{1}$$

where E_s and E_{sT} are the elastic modulus of unexposed and exposed structural steel, respectively, T_{max} is the maximum temperature achieved during the exposure. For reinforcing bars, E_s and E_{sT} in Eq.(1) need to be substituted by E_b and E_{bT} respectively.

The residual yield strength of structural steel and reinforcing bars after fire exposure are determined as follows [32]:

$$f_{yT} = \begin{cases} f_y & T_{max} \leq 500^{o}C \\ [1-2.33\times10^{-4}(T_{max}-500)-3.88\times10^{-7}(T_{max}-500)^2]f_y & T_{max} > 500^{o}C \end{cases} \tag{2}$$

$$f_{bT} = \begin{cases} f_b & T_{max} \leq 500^{o}C \\ [1-5.82\times10^{-4}(T_{max}-500)]f_b & T_{max} > 500^{o}C \end{cases} \tag{3}$$

where f_y and f_{yT} are the yield strength of unexposed and exposed structural steel, respectively, f_b and f_{bT} are the yield strength of unexposed and exposed reinforcing bars, respectively.

The model of concrete compressive stress-strain relationship proposed by Han et al. [33] is used in this study, which is a general stress-strain relationship model that has been widely used for simulation of square shaped concrete-filled steel tubular columns [33-36]. The equations are given as follows:

$$y=\begin{cases} 2x-x^2 & x\le 1 \\ \dfrac{x}{\beta_0(x-1)^{\eta}+x} & x>1 \end{cases} \tag{4}$$

in which $x=\varepsilon/\varepsilon_0$, $y=\sigma/\sigma_0$, $\xi=f_y A_s/f_{ck}A_c$, $\sigma_0=f_c^{'}$, $\varepsilon_0=\varepsilon_c^{'}+800\xi^{0.2}\times10^{-6}$, $\varepsilon_c^{'}=(1300+12.5f_c^{'})\cdot10^{-6}$, $\beta_0=(f_c^{'})^{0.1}\Big/\left(1.2\sqrt{1+\xi}\right)$, where A_s is the cross-sectional area of steel, A_c is the cross-sectional area of concrete, $f_c^{'}$ is the concrete cylinder strength, f_{ck} is the characteristic concrete strength (f_{ck}=0.67 f_{cu}, in which f_{cu} is the concrete cube strength), E_c is the elastic modulus and $E_c=4700\sqrt{f_c^{'}}$ N/mm^2 [37].

The residual elastic modulus E_{cT}, the residual compressive strength $f_{cT}^{'}$ and corresponding strain $\varepsilon_{cT}^{'}$ of concrete after exposure are determined as follows [38]:

$$E_{cT}=E_c\frac{f_{cT}^{'}/\varepsilon_{cT}^{'}}{f_c^{'}/\varepsilon_c^{'}} \tag{5}$$

$$f_{cT}^{'}=\frac{f_c^{'}}{1+2.4(T_{max}-20)^6\times10^{-17}} \tag{6}$$

$$\varepsilon_{cT}^{'}=\varepsilon_c^{'}[1+(1500T_{max}+5T_{max}^2)\times10^{-6}] \tag{7}$$

The stress-strain relationship in tension was assumed to be linear before and after the peak stress [16], given as follows:

$$\sigma=\begin{cases} E_{cT}\varepsilon & \varepsilon\le\varepsilon_{cr} \\ f_{tT}^{'}\left(\dfrac{\varepsilon-\varepsilon_{tu}}{\varepsilon_{cr}-\varepsilon_{tu}}\right) & \varepsilon_{cr}<\varepsilon\le\varepsilon_{tu} \\ 0 & \varepsilon>\varepsilon_{tu} \end{cases} \tag{8}$$

where $f_{tT}^{'}=0.1f_{cT}^{'}$, $\varepsilon_{cr}=f_{tT}^{'}\big/E_{cT}$, $\varepsilon_{tu}=15\varepsilon_{cr}$.

3.3 Verification of the FE model

The FE models were validated against the test results in this study. FE prediction and test results in terms of temperature distribution in specimens are shown in Fig.12, proving that the FE model could accurately predict the development of temperature in this kind of column. The measured and predicted average maximum temperatures in the specimens are compared in Table 6, in which d is the distance from the point of temperature measurement to the outer surface of the steel tube. The FE model yields pretty good predictions of the peak temperature attained during the exposure process.

Fig.13 presents the FE predictions and test results of load - axial displacement curves. The FE model was also validated against the unexposed square STCRC columns tested by Gan [8] and Liu et al. [9], as shown in Fig.14. The FE model generally yields good predictions, whereas there are some discrepancies between predictions and test results of stiffness for some specimens in Fig.13. These discrepancies may be due to measurement errors in this test. The FE predictions and test results of load-bearing capacities of the specimens are compared in Fig.15. The mean of the ratio of the FE to test results is 1.008 and corresponding standard deviation is 0.054, which confirms that the FE model can capture response of the square STCRC columns accurately.

4. Parametric studies and design recommendation

Parametric studies were performed to further investigate influences of parameters on the residual behaviour of square STCRC columns after fire exposure, including heating time t_h, width of square section B, yield strengths of structural steel f_y, yield strengths of reinforcing bar f_b and concrete strength f_c, steel tube to concrete area ratio α_s and reinforcement ratio α_b. These parameters were varied as: t_h=0 - 180 min, B=200 - 2000 mm, f_c'=24 - 50 N/mm^2, f_y=235 - 420 N/mm^2, f_b=335 - 500 N/mm^2, α_s=2.0% - 4.0%, α_b=2.0% - 5.0%.

Influences of these parameters on the residual cross-sectional capacity of square STCRC columns are shown in Fig.16. Load-bearing capacity declines with increasing heating time, whereas it increases significantly with increasing cross-sectional dimension. And Load-bearing capacity increases with the increase of material strengths, steel tube to concrete area ratio and reinforcement ratio.

Similar to cross-sectional capacity, the compressive stiffness also decreases with increase of heating time, whereas it increases significantly with increasing cross-sectional dimension, as shown in Fig.17.

Degradation of compressive stiffness is more severe than load-bearing capacity for columns after exposure.

A design method was proposed by Wang [39] for calculating cross-sectional capacity of square STCRC columns at room temperature, given as follows:

$$N_{u} = f_{cc} A_{c} + f_{b} A_{b} \tag{9}$$

where f_{cc} is the compressive strength of confined concrete and it can be calculated by Eq.(11), f_{b} is the yield strength of reinforcement, A_{c} and A_{b} are area of concrete and reinforcing bars, respectively.

$$f_{cc} = f_{c}' + 5.1 f_{el} \tag{10}$$

where f_{c}' is the concrete cylinder strength, f_{el} is the effective confining stress and it can be obtained by:

$$f_{el} = \frac{2 k_{s} k_{h} t_{s} f_{y}}{B} \tag{11}$$

where B is the width of square section, t_{s} is the thickness of steel tube, f_{y} is the yield strength of steel tube, k_{s} is a reduction factor of transverse stress of square section, k_{h} is a factor accounting for variation of transverse stress of steel tube in vertical direction.

$$k_{s} = -0.008 \frac{B}{t_{s}} - 0.090 \frac{f_{y}}{f_{c}'} + 0.036 \sqrt{\frac{B f_{y}}{t_{s} f_{c}'}} + 0.95 \tag{12}$$

$$k_{h} = -0.1 \frac{h_{t}}{B} + 1 \geq 0.5 \tag{13}$$

where h_{t} is the height of steel tube.

Consistent with the method above, a design method is proposed for evaluating cross-sectional capacity of square STCRC columns after fire exposure.

$$N_{uT} = f_{ccT,eq} A_{c} + f_{bT} A_{b} \tag{14}$$

where $f_{ccT,eq}$ is the equivalent compressive strength of confined concrete after fire exposure and f_{bT} is yield strength of reinforcement after exposure.

$$f_{ccT,eq} = f_{cT,eq}' + 5.1 f_{elT} \tag{15}$$

$$f_{\mathrm{cT,eq}}{}' = k\left[1 - \left(\frac{0.066}{B} - 0.007\right)t_{\mathrm{h}}\right]f_{\mathrm{c}}' \tag{16}$$

$$f_{\mathrm{elT}} = \frac{2k_{\mathrm{s}}k_{\mathrm{h}}t_{\mathrm{s}}f_{\mathrm{yT}}}{B} \tag{17}$$

$$f_{\mathrm{yT}} = \left(0.02t_{\mathrm{h}}^{2} - 0.15t_{\mathrm{h}} + 1.0\right)f_{\mathrm{y}} \tag{18}$$

$$f_{\mathrm{bT}} = \begin{cases} f_{\mathrm{b}} & t_{\mathrm{h}} \le 1.0 \\ \left(1.067 - 0.067t_{\mathrm{h}}\right)f_{\mathrm{b}} & 1.0 < t_{\mathrm{h}} \le 3.0 \end{cases} \tag{19}$$

where $f_{\mathrm{cT,eq}}{}'$ is the equivalent compressive strength of concrete after exposure, f_{yT} and f_{bT} are yield strength of structural steel and reinforcement after exposure, respectively, t_{h} is heating time in hours and B is width of square section in meters, k is a parameter introduced to consider influence of delay of temperature rise in concrete, which is recommend to be 0.98 for exposed columns. The factor k equals to 1.0 for unexposed columns.

A design method is also proposed for calculating compressive stiffness of square STCRC columns, given as follows:

$$EA = E_{\mathrm{cT,eq}}A_{\mathrm{c}} + E_{\mathrm{bT}}A_{\mathrm{b}} \tag{20}$$

$$E_{\mathrm{cT,eq}} = k \times \left[1 - \left(0.35 - 0.024t_{\mathrm{h}}\right)\sqrt{\frac{t_{\mathrm{h}}}{B}}\right]E_{\mathrm{c}} \tag{21}$$

$$E_{\mathrm{c}} = 4700\sqrt{f_{\mathrm{c}}'} \tag{22}$$

$$E_{\mathrm{bT}} = \begin{cases} E_{\mathrm{b}} & t_{\mathrm{h}} \le 1.0 \\ (1.015 - 0.015t_{\mathrm{h}})E_{\mathrm{b}} & 1.0 < t_{\mathrm{h}} \le 3.0 \end{cases} \tag{23}$$

where $E_{\mathrm{cT,eq}}$ is the equivalent elastic modulus of exposed concrete, E_{bT} is the elastic modulus of reinforcement, t_{h} is heating time in hours and B is width of square section in meters.

Comparisons of predicted residual cross-sectional capacity between FE results and design method are presented in Fig.18 (a), and compressive stiffness results are shown in Fig.18 (b). The mean of the ratio of design method to FE results according to residual capacity is 1.056 and corresponding standard deviation is 0.047, whereas the mean of the ratio of design method to FE results of compressive stiffness is 1.014 and corresponding standard deviation is 0.065.

The residual capacity and compressive stiffness of specimens tested in this study and literatures [8, 9] were also predicted using recommended design method and are presented in Fig.19. The recommended design method yields reasonable predictions for both residual cross-sectional capacity and compressive stiffness, though there are some differences for the compressive stiffness.

5. Conclusions

Eighteen square STCRC stub columns were tested to study the fundamental performance of these columns after fire exposure. Heating time (0 min, 45 min and 90 min) and cross-section dimension (B=200 mm and 250 mm) were varied in the test. A FE model was established using program ABAQUS and were employed to extend ranges of studied parameters. Influences of heating time, cross-sectional dimension, material strengths, steel tube to concrete area ratio and reinforcement ratio on load-bearing capacity and compressive stiffness were analysed and discussed. Based on experimental and numerical results, a design method was proposed for evaluating residual cross-sectional capacity and compressive stiffness of square STCRC columns after fire exposure. The following conclusions can be drawn from this study:

(1) Failure modes of square STCRC columns may change after fire exposure. The unexposed and the exposed columns with heating time of 45 min failed by shear failure, whereas the columns with heating time of 90 min failed by outward buckling of steel tube and crushing of concrete in this test. Degradation of concrete strength after exposure is irreversible, whereas steel strength could partially recover after cooing to room temperature, and thus the effect of confinement of steel tube to concrete increases relatively. Therefore ductility of columns enhances with increasing heating time and failure modes changes.

(2) Longer heating time results in lower residual load-bearing capacity and compressive stiffness due to the decrease of strength and elastic modulus after fire exposure. Reduction of stiffness is more severe than that of load-bearing capacity, consistent with influences of elevated temperatures on material properties. With increase of cross-sectional dimension, strengths of materials, steel tube to concrete area ratio and reinforcement ratio, the load-bearing capacity and compressive stiffness increases correspondingly.

(3) A design method was proposed for calculating residual cross-sectional capacity and compressive

stiffness of square STCRC columns after fire exposure, which can be used for damage evaluation of this kind of column after fire exposure.

6. Acknowledgements

The research presented in this paper was sponsored by the National Natural Science Foundation (51508131), China Postdoctoral Science Foundation (2016M591535) and the Fundamental Research Funds for the Central Universities (HIT.NSRIF.201860); their financial support is highly appreciated.

7. References

[1] X. Wang, J. Liu, Behavior and design of slender square tubed-reinforced-concrete columns subjected to eccentric compression, Thin-Walled Structures 120 (2017) 153-160.

[2] M. Tomii, K. Sakino, K. Watanabe, Y. Xiao, Lateral load capacity of reinforced concrete short columns confined by steel tube, Proceeding of International Speciality Conference on Concrete Filled Steel Tubular Structures, Harbin, China., 1985, pp. 19-26.

[3] M. Tomii, K. Sakino, Y. Xiao, K. Watanabe, Earthquake resisting hysteretic behavior of reinforced concrete short columns confined by steel tube, Proceeding of International Speciality Conference on Concrete Filled Steel Tubular Structures, Harbin, China., 1985, pp. 119-125.

[4] K. Sakino, M. Tomii, K. Watanabe, Sustaining load capacity of plain concrete stub columns by circular steel tubes, Proceeding of International Speciality Conference on Concrete Filled Steel Tubular Structures, Harbin, China., 1985, pp. 112-118.

[5] L.-H. Han, G.-H. Yao, Z.-B. Chen, Q. Yu, Experimental behaviours of steel tube confined concrete (STCC) columns, Steel and Composite Structures 5(6) (2005) 459-484.

[6] J. Liu, X. Zhou, Behavior and strength of tubed RC stub columns under axial compression, Journal of Constructional Steel Research 66(1) (2010) 28-36.

[7] Q. Yu, Z. Tao, W. Liu, Z.-B. Chen, Analysis and calculations of steel tube confined concrete (STCC) stub columns, Journal of Constructional Steel Research 66(1) (2010) 53-64.

[8] D. Gan, Static and seismic behavior of steel tube confined concrete short columns, Lanzhou University (2012) (in Chinese).

[9] J. Liu, X. Wang, S. Zhang, Behavior of square tubed reinforced-concrete short columns subjected

to eccentric compression, Thin-Walled Structures 91(0) (2015) 108-115.
[10] X. Wang, J. Liu, S. Zhang, Behavior of short circular tubed-reinforced-concrete columns subjected to eccentric compression, Engineering Structures 105 (2015) 77-86.
[11] X. Zhou, J. Liu, X. Wang, Y.F. Chen, Behavior and design of slender circular tubed-reinforced-concrete columns subjected to eccentric compression, Engineering Structures 124 (2016) 17-28.
[12] R. Aboutaha, R. Machado, Seismic resistance of steel-tubed high-strength reinforced-concrete columns, Journal of Structural Engineering 125(5) (1999) 485-494.
[13] L.-H. Han, H. Qu, Z. Tao, Z.-F. Wang, Experimental behaviour of thin-walled steel tube confined concrete column to RC beam joints under cyclic loading, Thin-walled structures 47(8) (2009) 847-857.
[14] X. Zhou, J. Liu, Seismic behavior and shear strength of tubed RC short columns, Journal of Constructional Steel Research 66(3) (2010) 385-397.
[15] J. Liu, J. Ali Abdullah, S. Zhang, Hysteretic behavior and design of square tubed reinforced and steel reinforced concrete (STRC and/or STSRC) short columns, Thin-Walled Structures 49(7) (2011) 874-888.
[16] F. Liu, L. Gardner, H. Yang, Post-fire behaviour of reinforced concrete stub columns confined by circular steel tubes, Journal of Constructional Steel Research 102(0) (2014) 82-103.
[17] H. Yang, F. Liu, L. Gardner, Post-fire behaviour of slender reinforced concrete columns confined by circular steel tubes, Thin-Walled Structures 87(0) (2015) 12-29.
[18] F. Liu, H. Yang, L. Gardner, Post-fire behaviour of eccentrically loaded reinforced concrete columns confined by circular steel tubes, Journal of Constructional Steel Research 122 (2016) 495-510.
[19] ISO 6892-1. Metallic materials Tensile testing Part 1: Method of test at room temperature, International Organization for Standardization (2009).
[20] L.T. Phan, N.J. Carino, Review of mechanical properties of HSC at elevated temperature, Journal of Materials in Civil Engineering 10(1) (1998) 58-64.
[21] M.S. Abrams, Compressive strength of concrete at temperatures to 1600F, (1973).

[22] K.D. Hertz, Concrete strength for fire safety design, Magazine of Concrete Research 57(8) (2005) 445-453.

[23] J. Huo, J. Zhang, Z. Wang, Y. Xiao, Effects of sustained axial load and cooling phase on post-fire behaviour of reinforced concrete stub columns, Fire Safety Journal 59(0) (2013) 76-87.

[24] ISO 834. Fire Resistance Tests-Elements of Building Construction, International Organization for Standardization (1975).

[25] H. Zhao, Y. Wang, F. Liu, Stress-strain relationship of coarse RCA concrete exposed to elevated temperatures, Magazine of Concrete Research 0(0) (2017) 1-16.

[26] Z. Tao, L.-H. Han, B. Uy, X. Chen, Post-fire bond between the steel tube and concrete in concrete-filled steel tubular columns, Journal of Constructional Steel Research 67(3) (2011) 484-496.

[27] T.T. Lie, Fire resistance of circular steel columns filled with bar-reinforced Concrete, Journal of Structural Engineering-ASCE 120(5) (1994) 1489-1509.

[28] J. Ding, Y.C. Wang, Realistic modelling of thermal and structural behaviour of unprotected concrete filled tubular columns in fire, Journal of Constructional Steel Research 64(10) (2008) 1086-1102.

[29] H. Lu, X.-L. Zhao, L.-H. Han, FE modelling and fire resistance design of concrete filled double skin tubular columns, Journal of Constructional Steel Research 67(11) (2011) 1733-1748.

[30] X. Lv, H. Yang, S. Zhang, Effect of contact thermal resistance on temperature distributions of concrete-filled steel tubes in fire, Journal of Harbin Institute of Technology 18(1) (2011) 81-88.

[31] N. AbdelRahman, K.S. Sivakumaran, Material properties models for analysis of cold-formed steel members, J Struct Eng-Asce 123(9) (1997) 1135-1143.

[32] Z. Tao, X. Wang, B. Uy, Stress-strain curves of structural and reinforcing steels after exposure to elevated temperatures, Journal of Materials in Civil Engineering 25(9) (2013) 1306-1316.

[33] L.-H. Han, G.-H. Yao, Z. Tao, Performance of concrete-filled thin-walled steel tubes under pure torsion, Thin-Walled Structures 45(1) (2007) 24-36.

[34] D. Lam, X.H. Dai, L.H. Han, Q.X. Ren, W. Li, Behaviour of inclined, tapered and STS square CFST stub columns subjected to axial load, Thin-Walled Structures 54(0) (2012) 94-105.

[35] Y.-F. Yang, Z.-C. Zhang, F. Fu, Experimental and numerical study on square RACFST members

under lateral impact loading, Journal of Constructional Steel Research 111(0) (2015) 43-56.

[36] M.F. Javed, N.H.R. Sulong, S.A. Memon, S.K.U. Rehman, N.B. Khan, FE modelling of the flexural behaviour of square and rectangular steel tubes filled with normal and high strength concrete, Thin-Walled Structures 119 (2017) 470-481.

[37] ACI 318-08, Building code requirements for structural concrete and commentary, American Concrete Institute (2008).

[38] Z. Guo, X. Shi, Experiment and calculation of reinforced concrete at elevated temperatures, Elsevier Inc.2011.

[39] X. Wang, Study on the behavior and strength of TRC and TSRC columns, Harbin Institute of Technology (2017) (in Chinese)

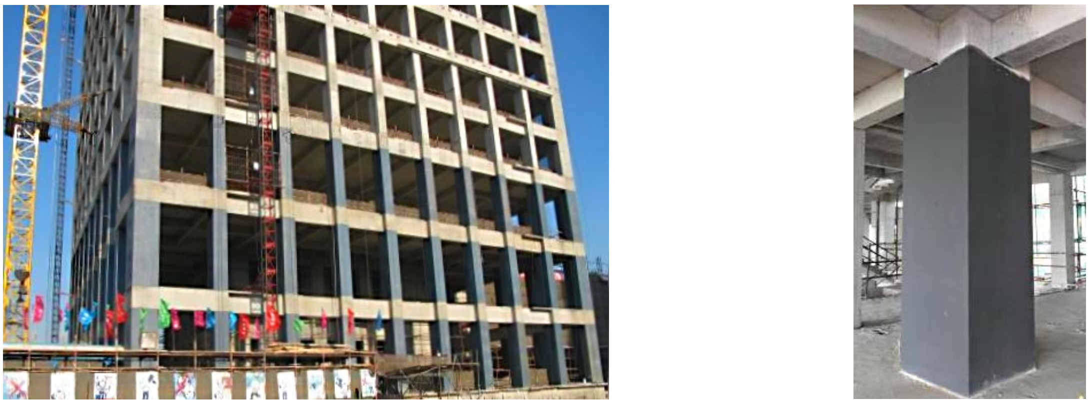

(a) (b)

Fig.1 A typical building using STCRC columns [1]: (a) STCRC columns in the bottom three stories; (b) details of a STCRC column.

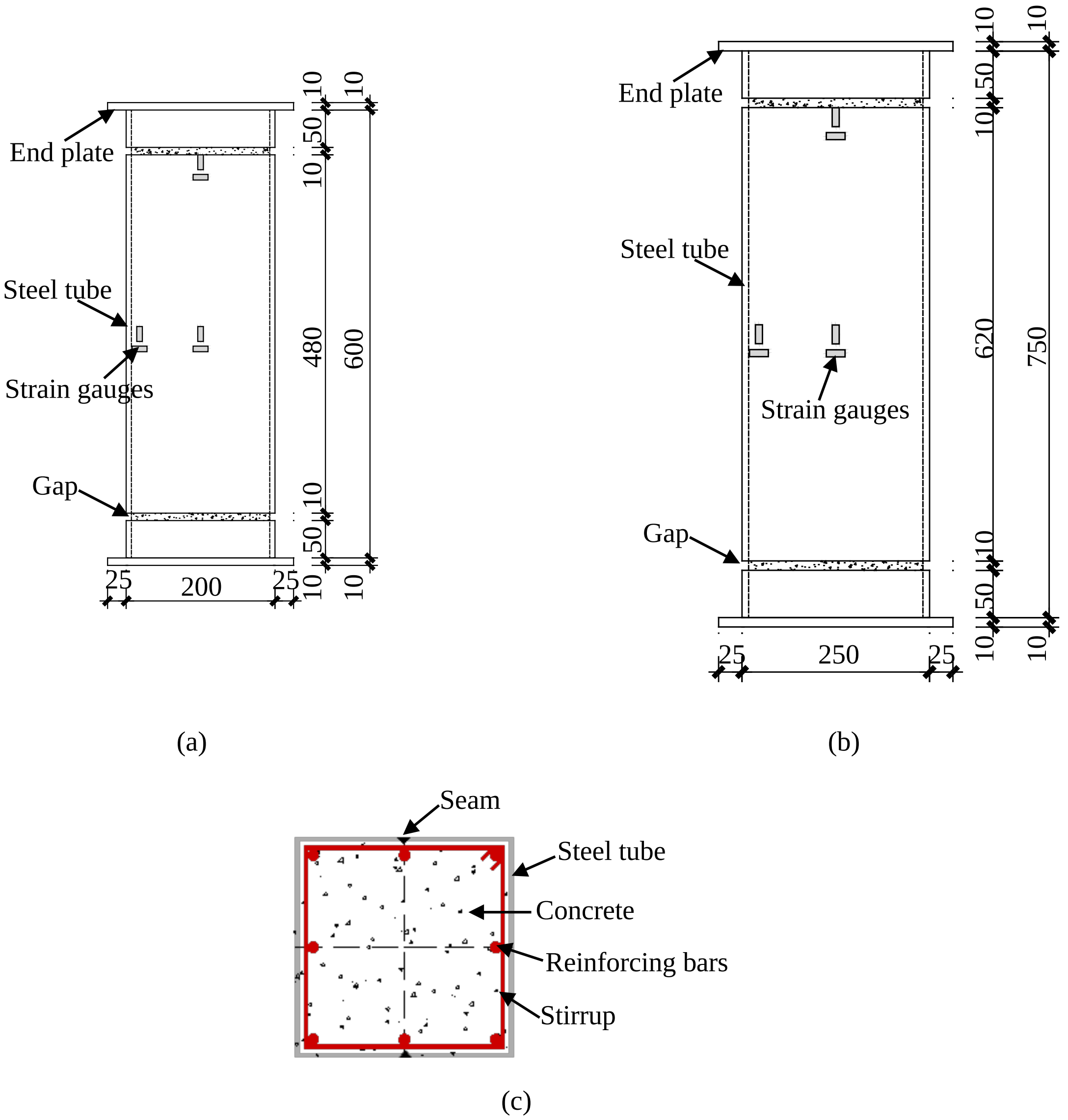

Fig.2 Details of specimens: (a) elevation of S200 specimen; (b) elevation of S250 specimen; and (c) cross-section (unit: mm).

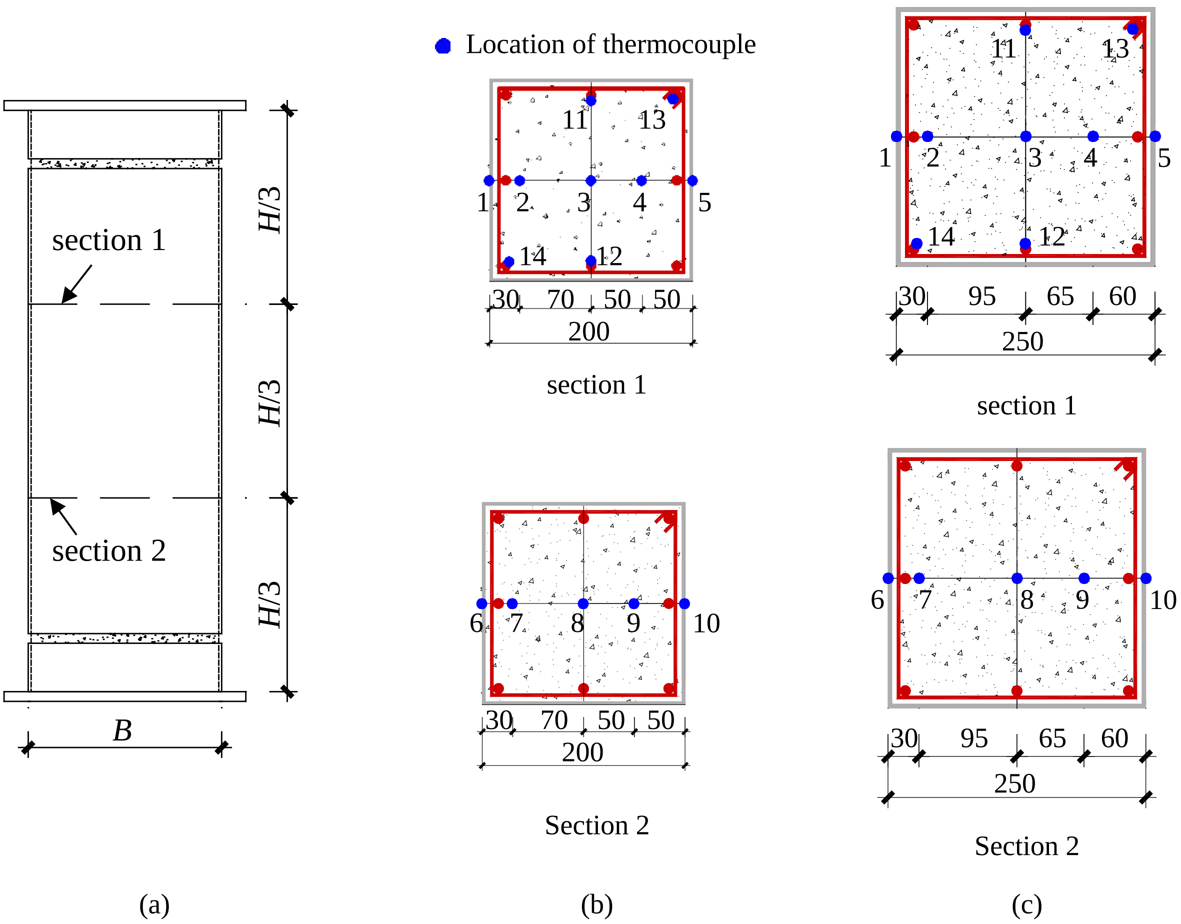

Fig.3 Layouts of thermocouples: (a) elevation; (b) S200-45min/90min; and (c) S250-45min/90min (unit: mm).

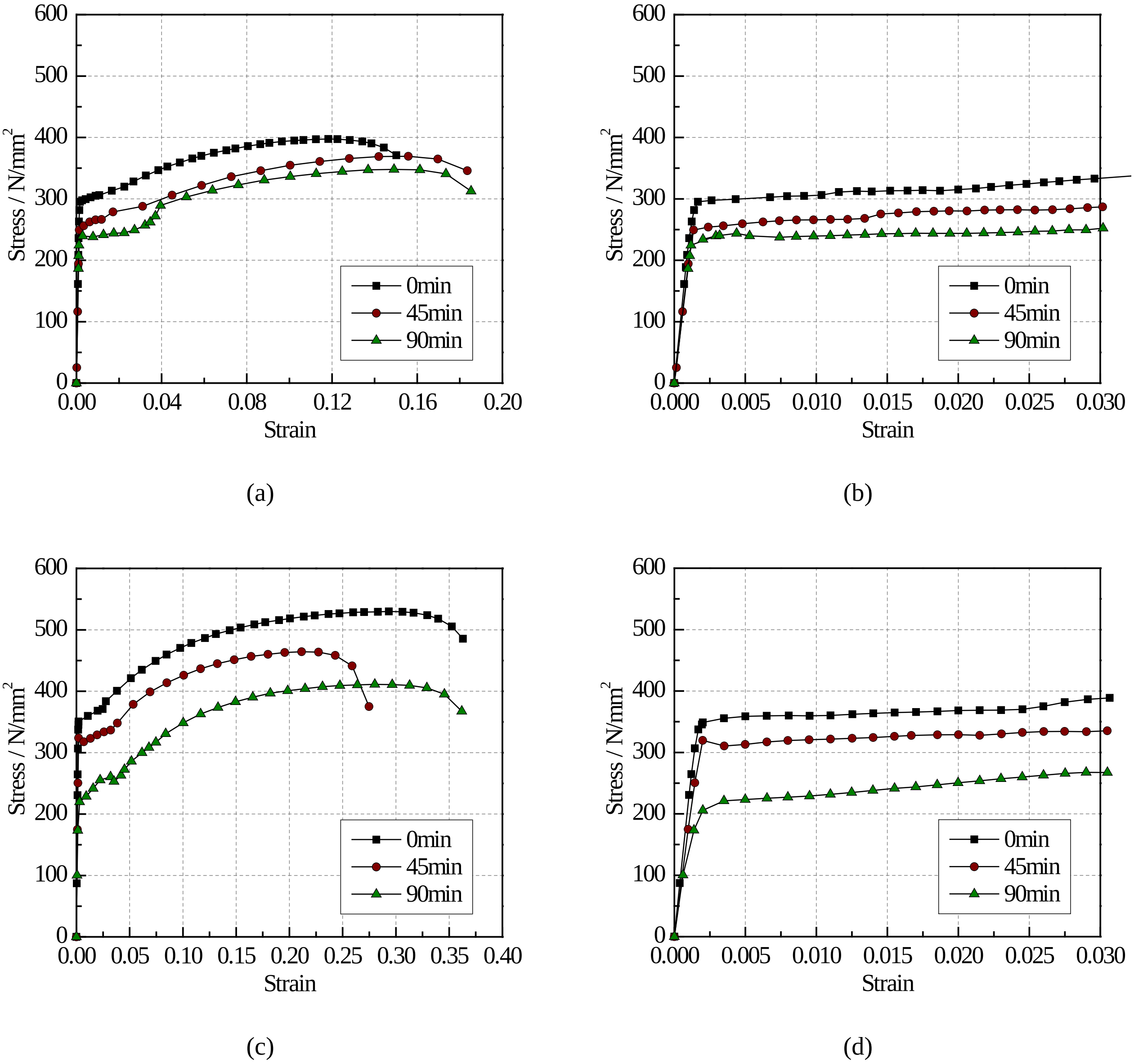

Fig.4 Stress-strain curves of steel tubes: (a) t_s=1.75mm; (b) partial enlargement of (a); (c) t_s=2.20mm; and (d) partial enlargement of (c).

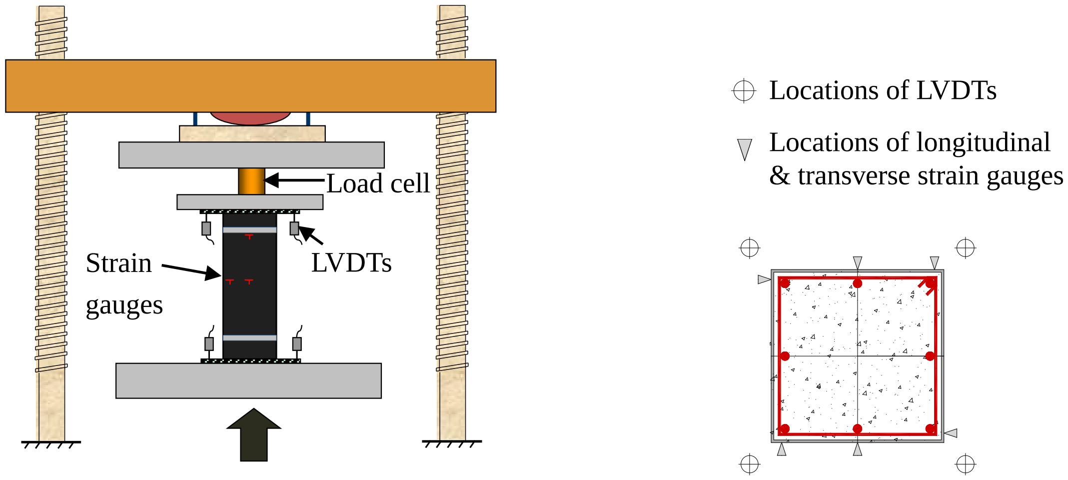

Fig.5 Layouts of instrumentations: (a) elevation; and (b) plan.

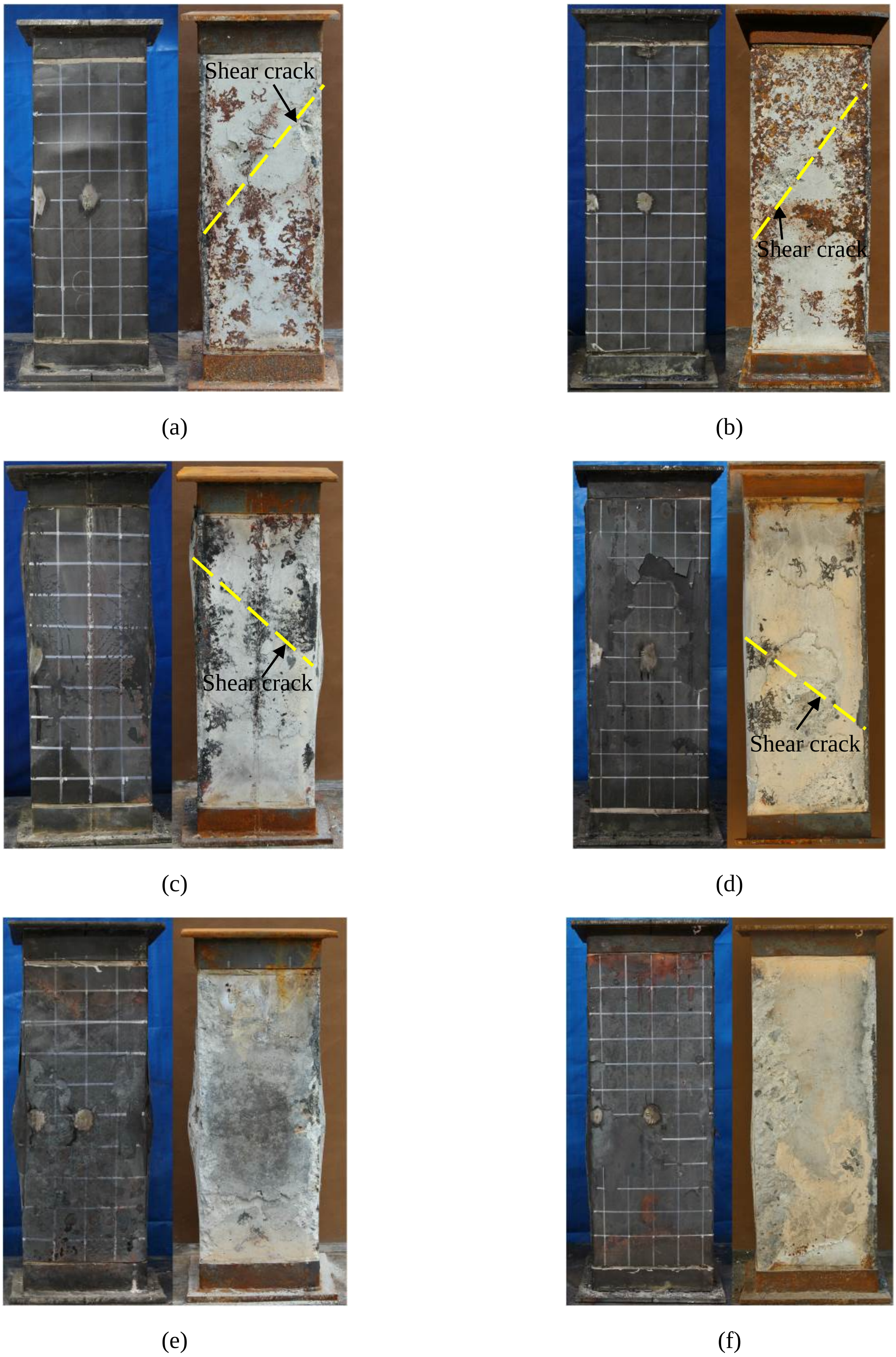

Fig.6 Typical failure modes of specimens: (a) S200-0; (b) S250-0; (c) S200-45; (d) S250-45; (e) S200-90; and (f) S250-90.

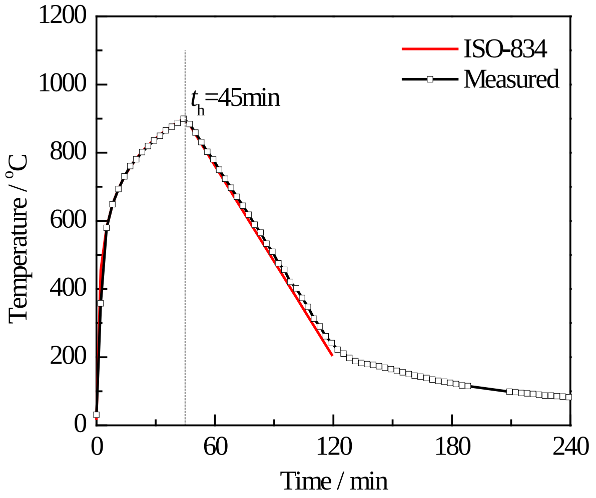

(a)

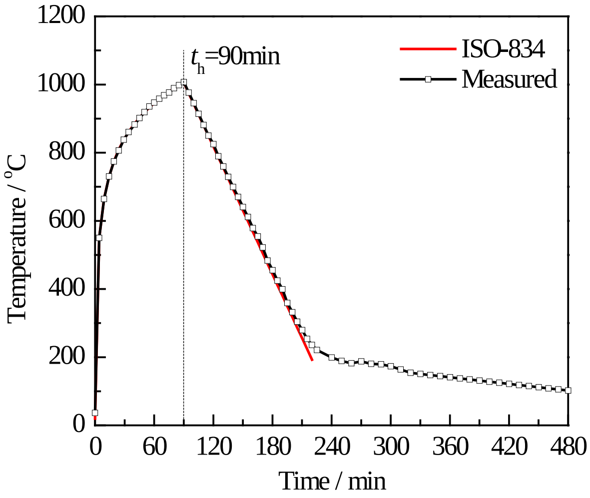

(b)

Fig.7 Comparisons between measured furnace temperature and ISO-834 standard fire curve: (a) 45min; and (b) 90min.

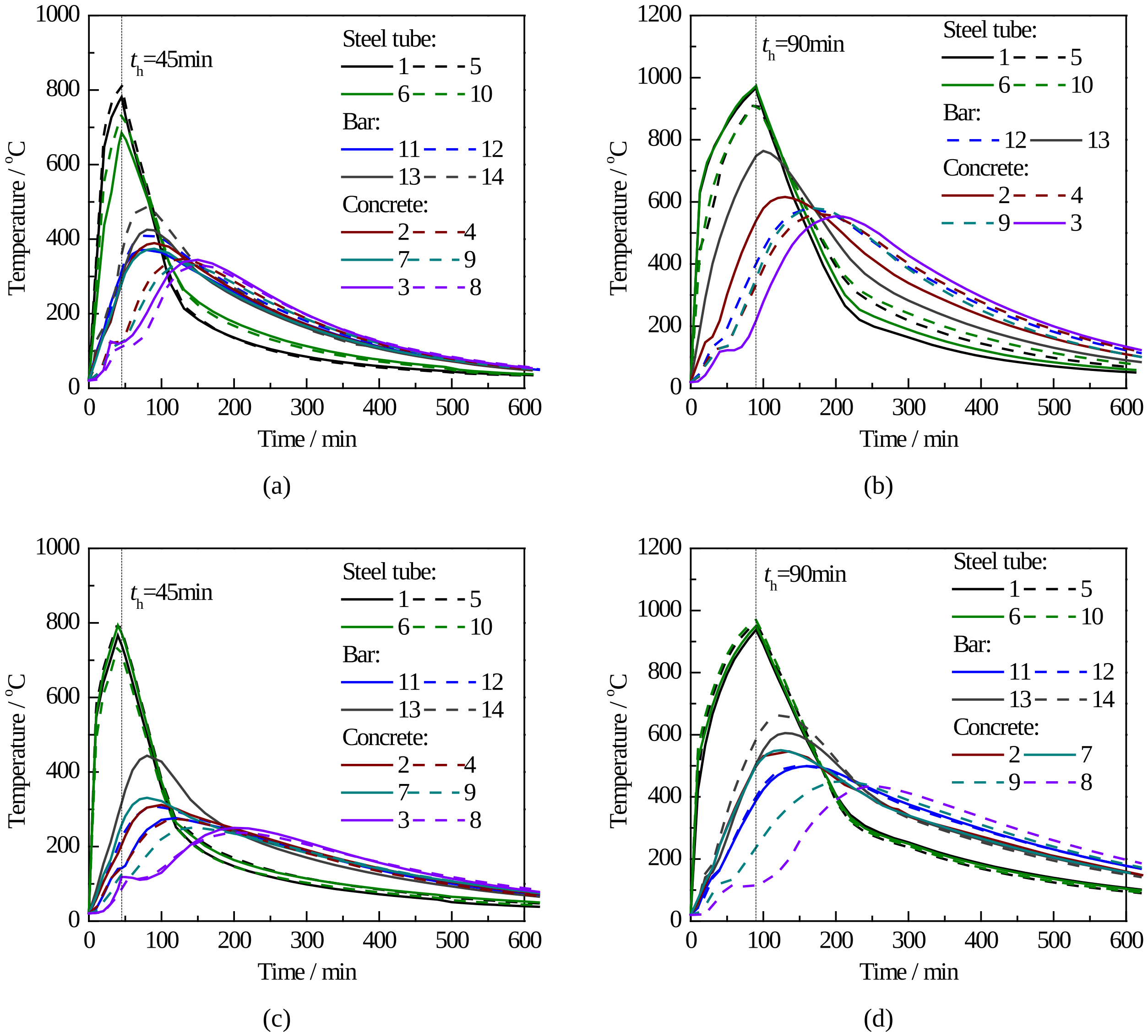

Fig.8 Measured cross-sectional temperatures of specimens: (a) S200-45min; (b) S200-90min; (c) S250-45min; and (d) S250-90min.

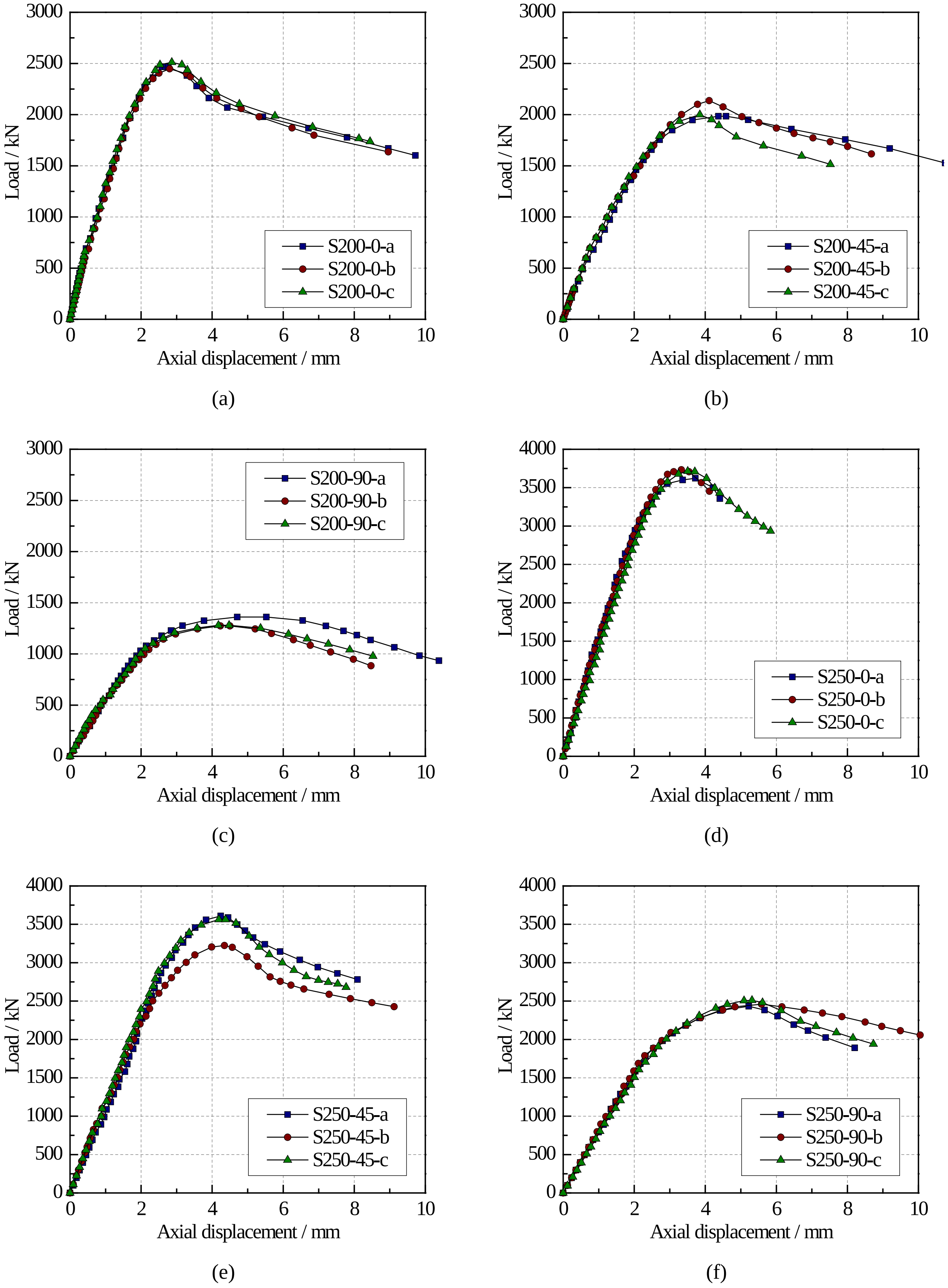

Fig.9 Axial load-displacement curves: (a) S200-0; (b) S200-45; (c) S200-90; (d) S250-0; (e) S250-45; and (f) S250-90.

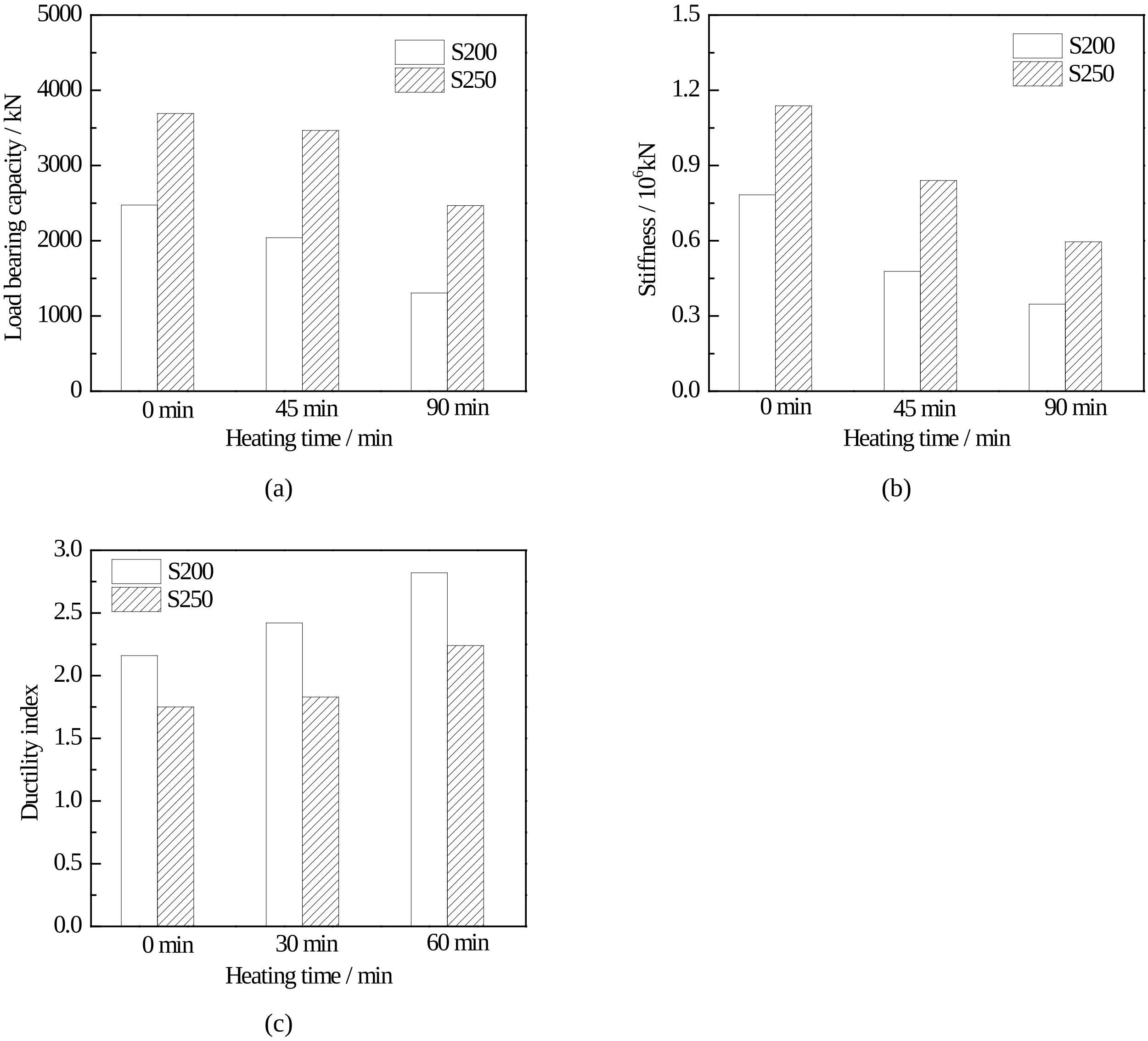

Fig.10 Influences of heating time on: (a) load bearing capacity; (b) stiffness; and (c) ductility index.

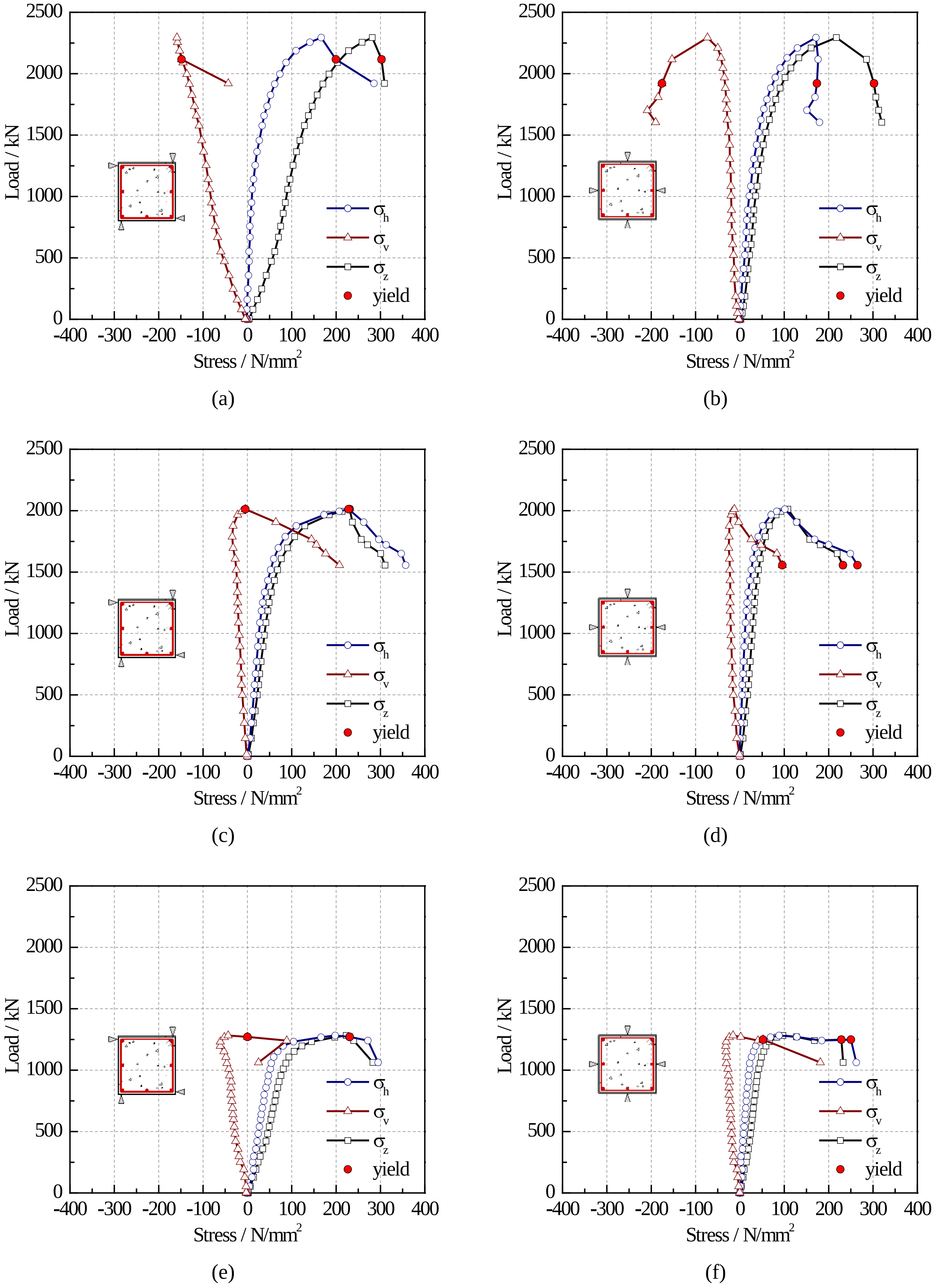

Fig.11 Axial load-steel tube stress curves: S200-0: (a) at corner; (b) middle; S200-45: (c) at corner; (d) middle; S200-90: (e) at corner; and (f) middle.

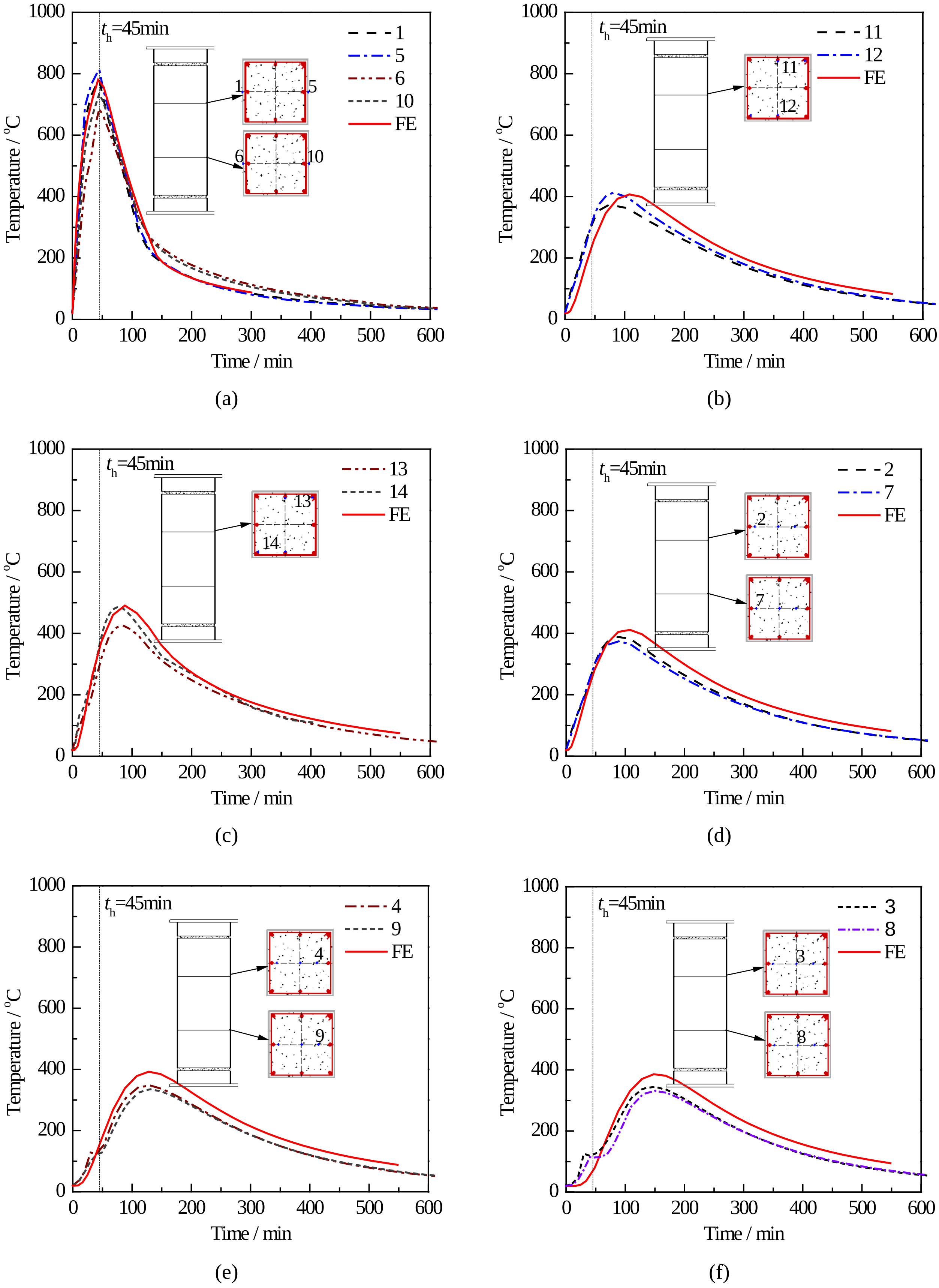

(a)
Temperature / °C
Time / min
t_h=45min
1
5
6
10
FE
(b)
Temperature / °C
Time / min
t_h=45min
11
12
FE
(c)
Temperature / °C
Time / min
t_h=45min
13
14
FE
(d)
Temperature / °C
Time / min
t_h=45min
2
7
FE
(e)
Temperature / °C
Time / min
t_h=45min
4
9
FE
(f)
Temperature / °C
Time / min
t_h=45min
3
8
FE

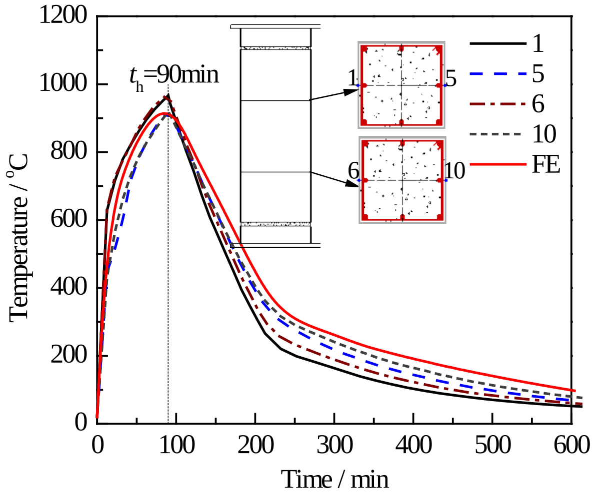

Temperature / °C
Time / min
t_h=90min
1
5
6
10
FE

(g)

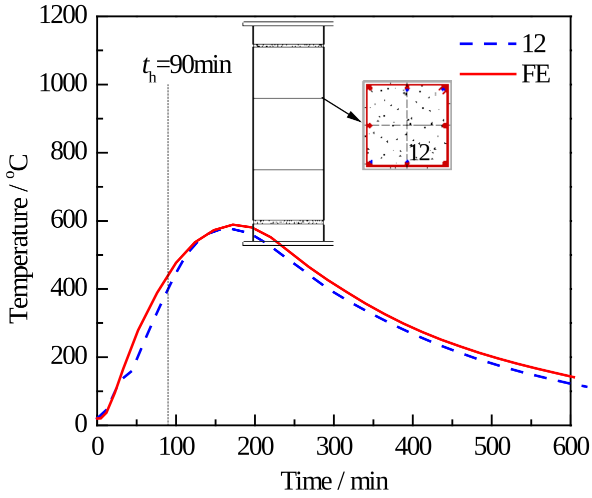

Temperature / °C
Time / min
t_h=90min
12
FE

(h)

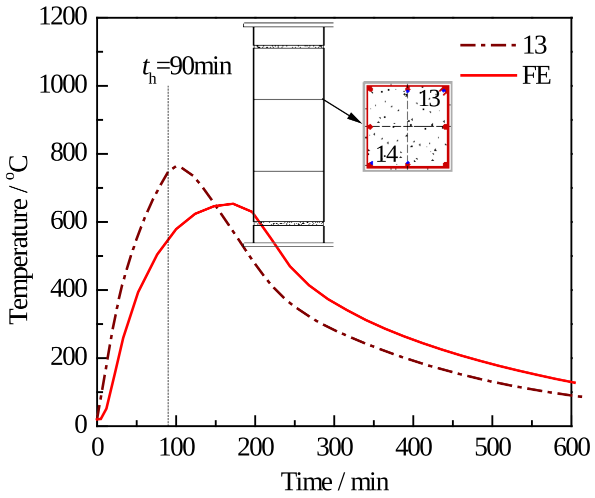

Temperature / °C
Time / min
t_h=90min
13
14
FE

(i)

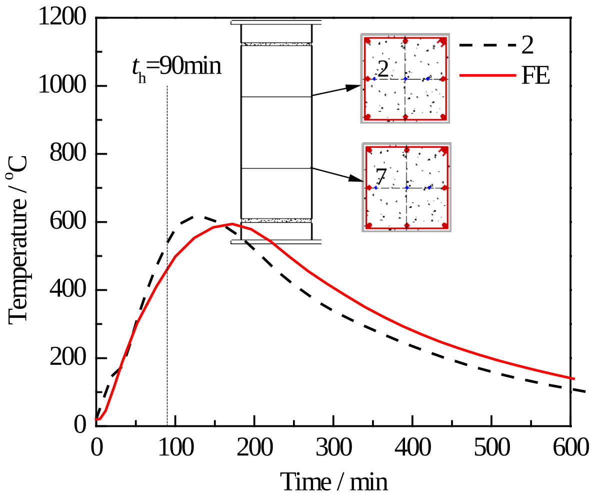

Temperature / °C
Time / min
t_h=90min
2
7
FE

(j)

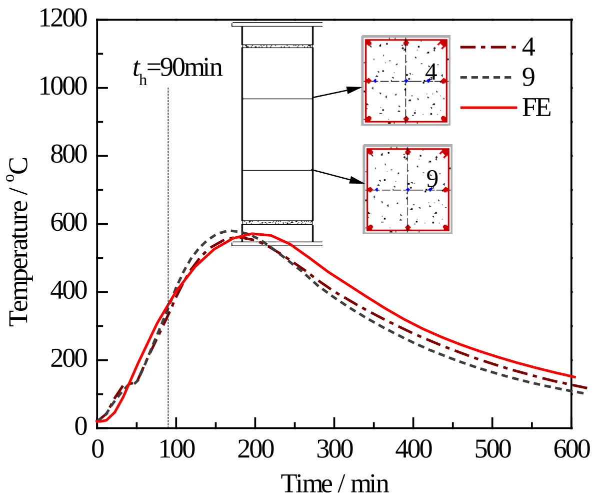

Temperature / °C
Time / min
t_h=90min
4
9
FE

(k)

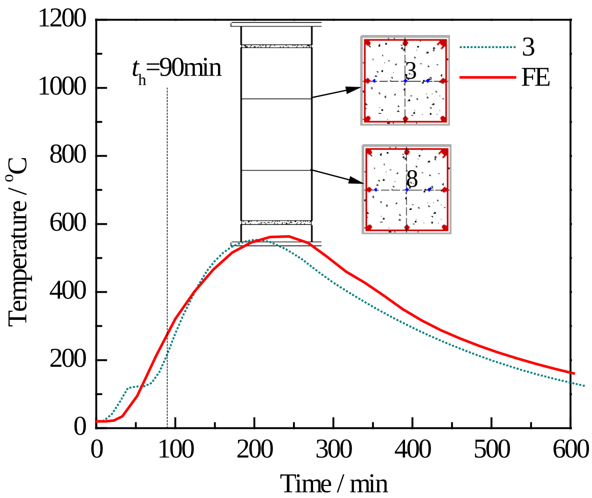

Temperature / °C
Time / min
t_h=90min
3
8
FE

(m)

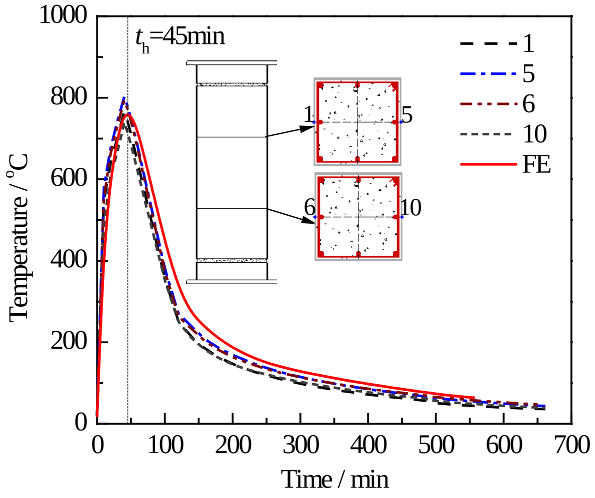

Temperature / °C
Time / min
t_h=45min
1
5
6
10
FE

(n)

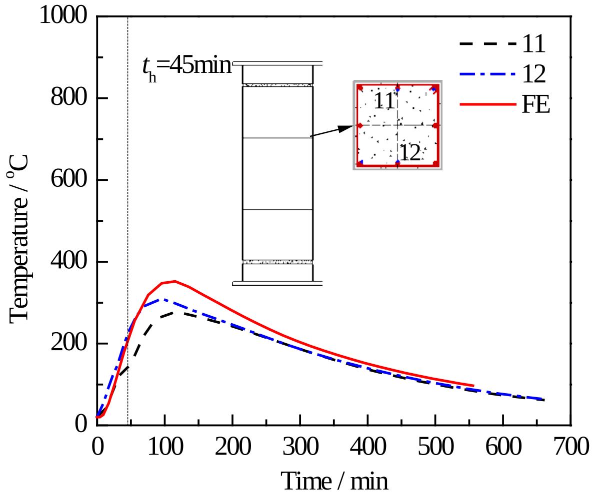

Temperature / °C
Time / min
t_h=45min
11
12
FE

(o)

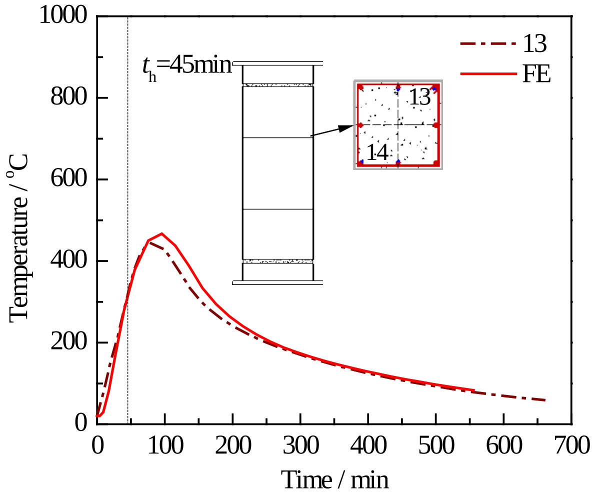

Temperature / °C
Time / min
t_h=45min
13
14
FE

(p)

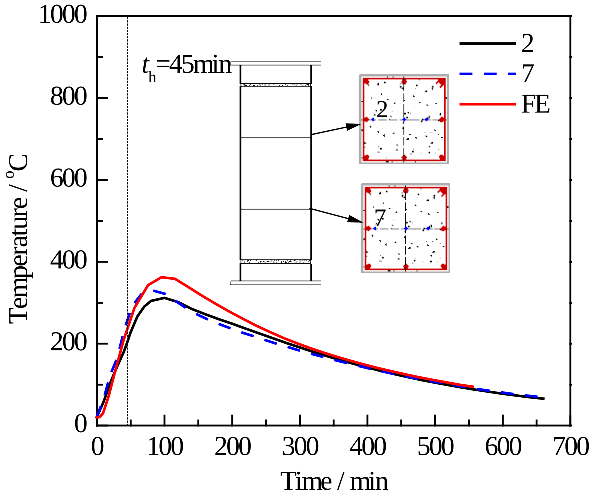

Temperature / °C
Time / min
t_h=45min
2
7
FE

(q)

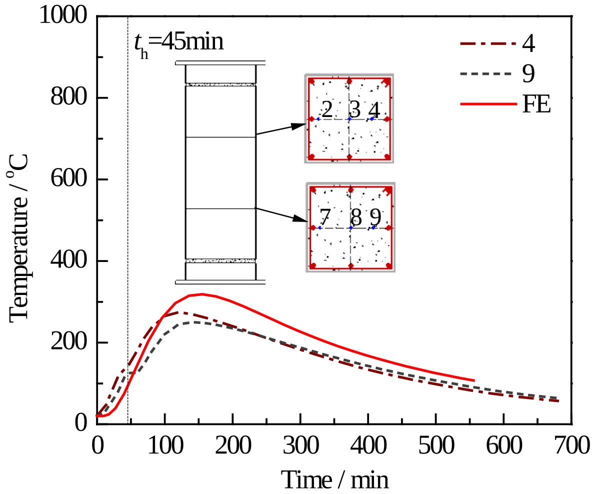

Temperature / °C
Time / min
t_h=45min
2 3 4
7 8 9
4
9
FE

(r)

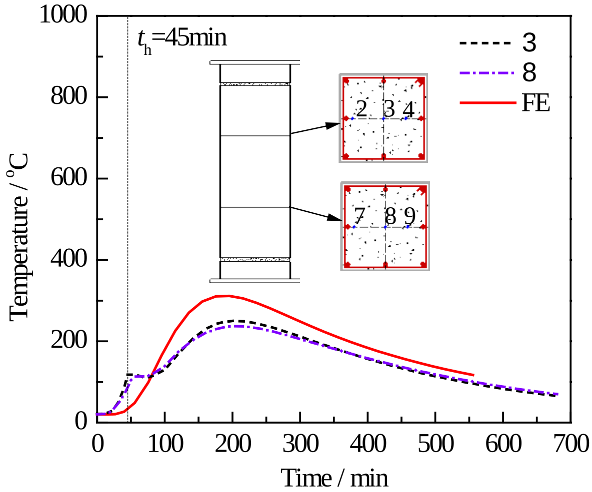

Temperature / °C
Time / min
t_h=45min
2 3 4
7 8 9
3
8
FE

(s)

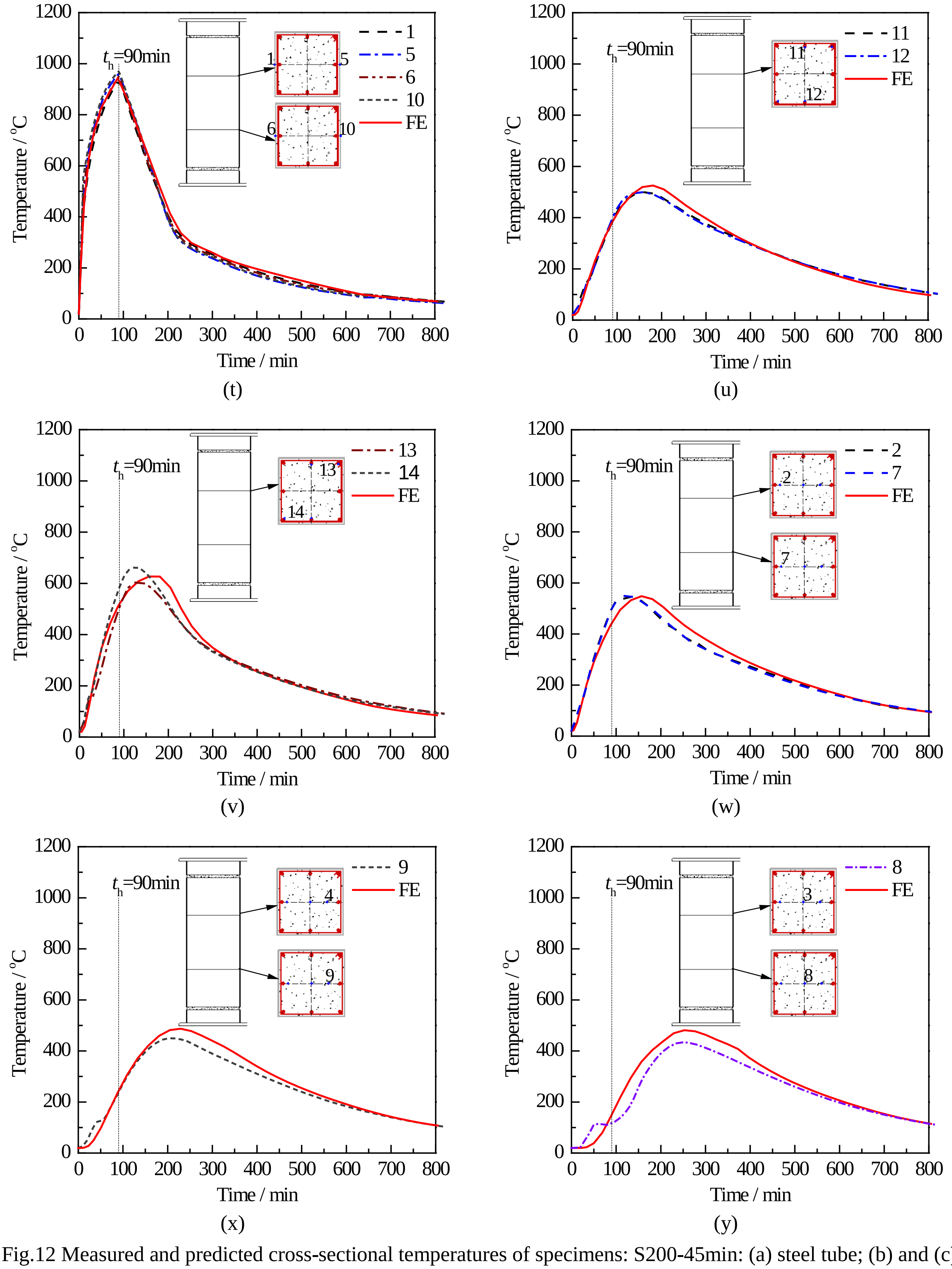

Fig.12 Measured and predicted cross-sectional temperatures of specimens: S200-45min: (a) steel tube; (b) and (c) reinforcement bars; (d) - (f) concrete; S200-90min: (g) steel tube; (h) and (i) reinforcement bars; (j) - (m) concrete; S250-45min: (n) steel tube; (o) and (p) reinforcement bars; (q) - (s) concrete; and S250-90min: (t) steel tube; (u) and (v) reinforcement bars; (w) - (y) concrete.

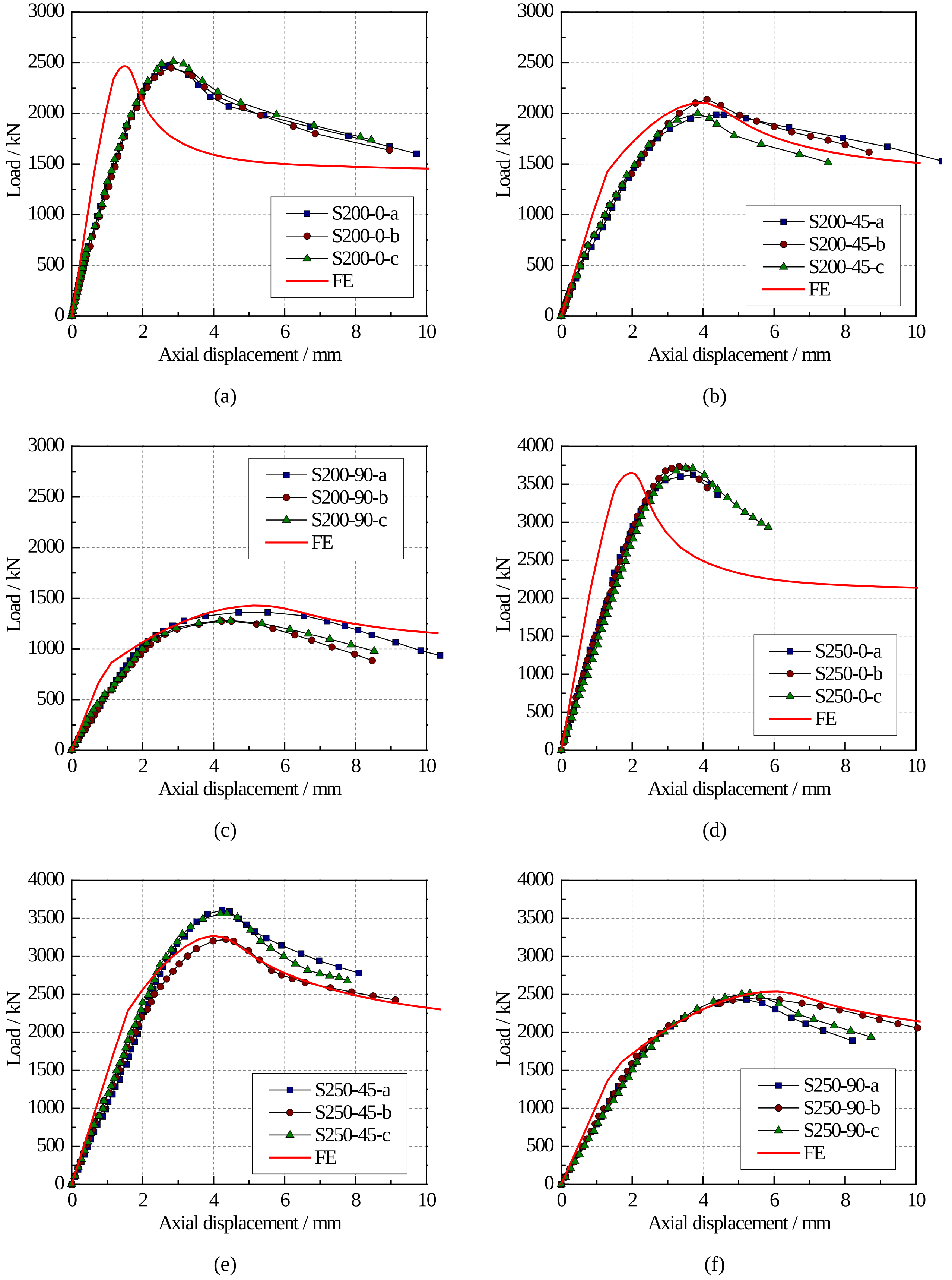

Fig.13 Comparisons of test and FE load - displacement curves of square STCRC stub columns after exposure: (a) S200-0; (b) S200-45; (c) S200-90; (d) S250-0; (e) S250-45; and (f) S250-90.

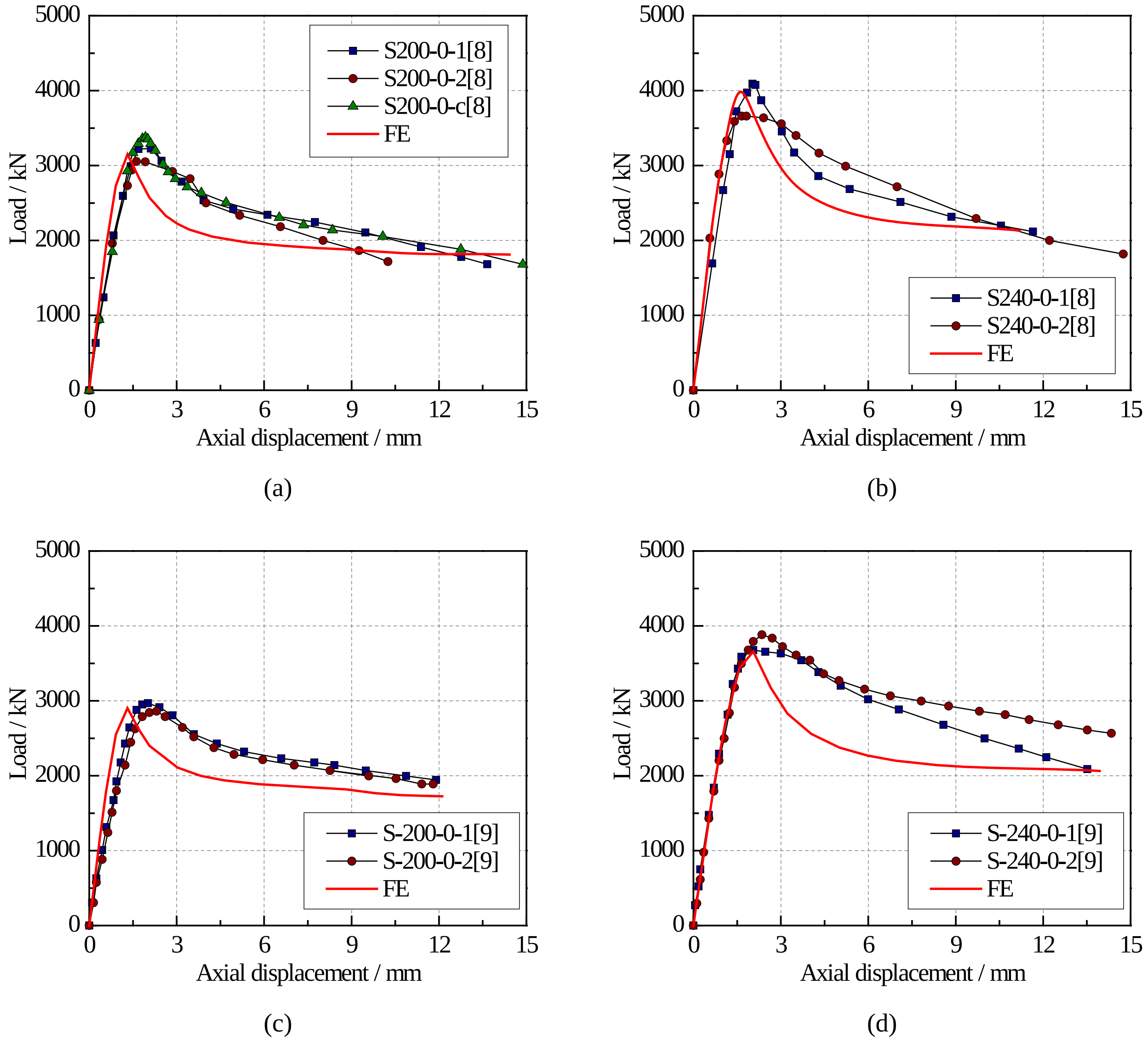

Fig.14 Comparisons of test and FE load - displacement curves of square STCRC stub columns at ambient temperature: (a) S200-0; (b) S240-0; (c) S-200-0; and (d) S-240-0.

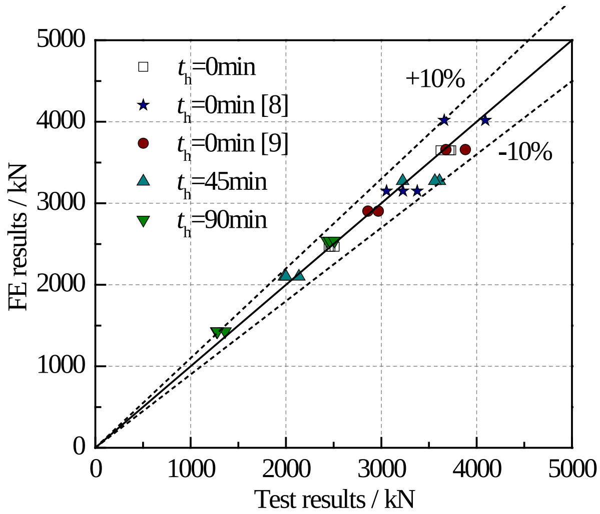

Fig.15 Comparisons of test and FE load - bearing capacities.

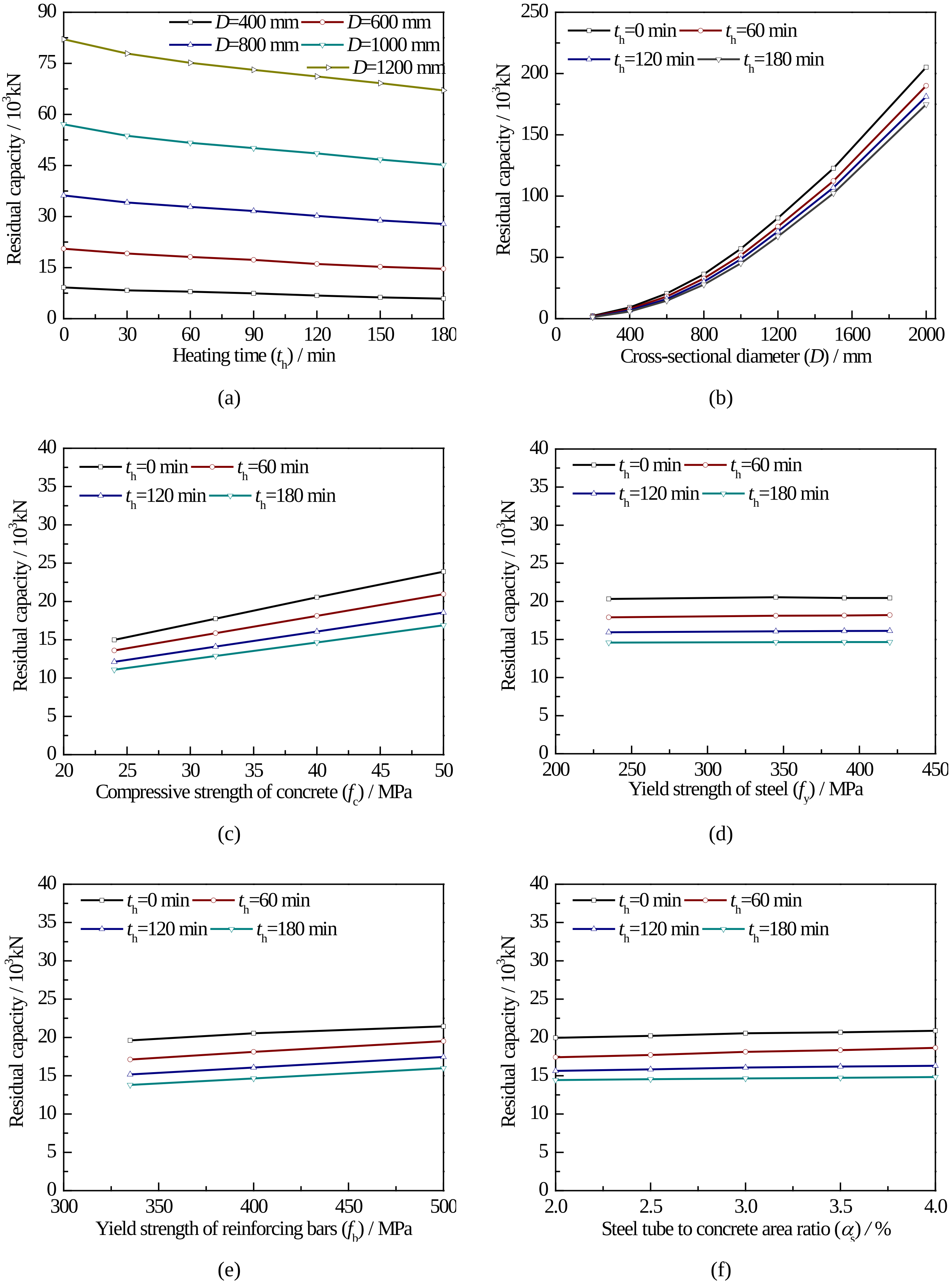
D=400 mm
D=600 mm
D=800 mm
D=1000 mm
D=1200 mm
Residual capacity / 10³kN
Heating time (tₕ) / min
(a)
tₕ=0 min
tₕ=60 min
tₕ=120 min
tₕ=180 min
Residual capacity / 10³kN
Cross-sectional diameter (D) / mm
(b)
tₕ=0 min
tₕ=60 min
tₕ=120 min
tₕ=180 min
Residual capacity / 10³kN
Compressive strength of concrete (f꜀) / MPa
(c)
tₕ=0 min
tₕ=60 min
tₕ=120 min
tₕ=180 min
Residual capacity / 10³kN
Yield strength of steel (fᵧ) / MPa
(d)
tₕ=0 min
tₕ=60 min
tₕ=120 min
tₕ=180 min
Residual capacity / 10³kN
Yield strength of reinforcing bars (f_b) / MPa
(e)
tₕ=0 min
tₕ=60 min
tₕ=120 min
tₕ=180 min
Residual capacity / 10³kN
Steel tube to concrete area ratio (αₛ) / %
(f)

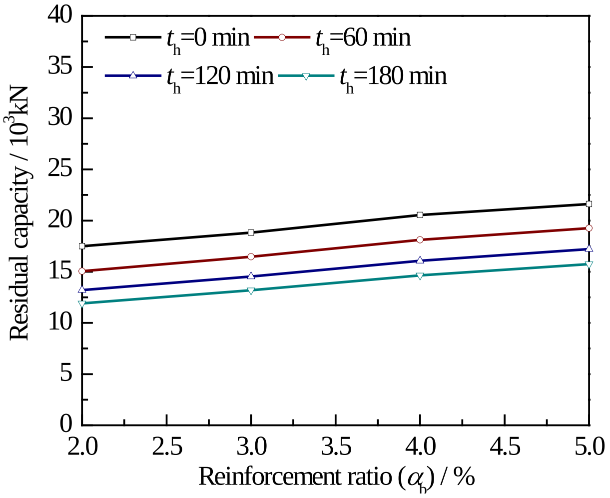

(g)

Fig.16 Influences of parameters on residual capacity: (a) heating time; (b) cross-sectional dimension; (c) compressive strength of concrete; (d) yield strength of steel; (e) yield strength of reinforcement; (f) steel ratio; and (g) reinforcement ratio.

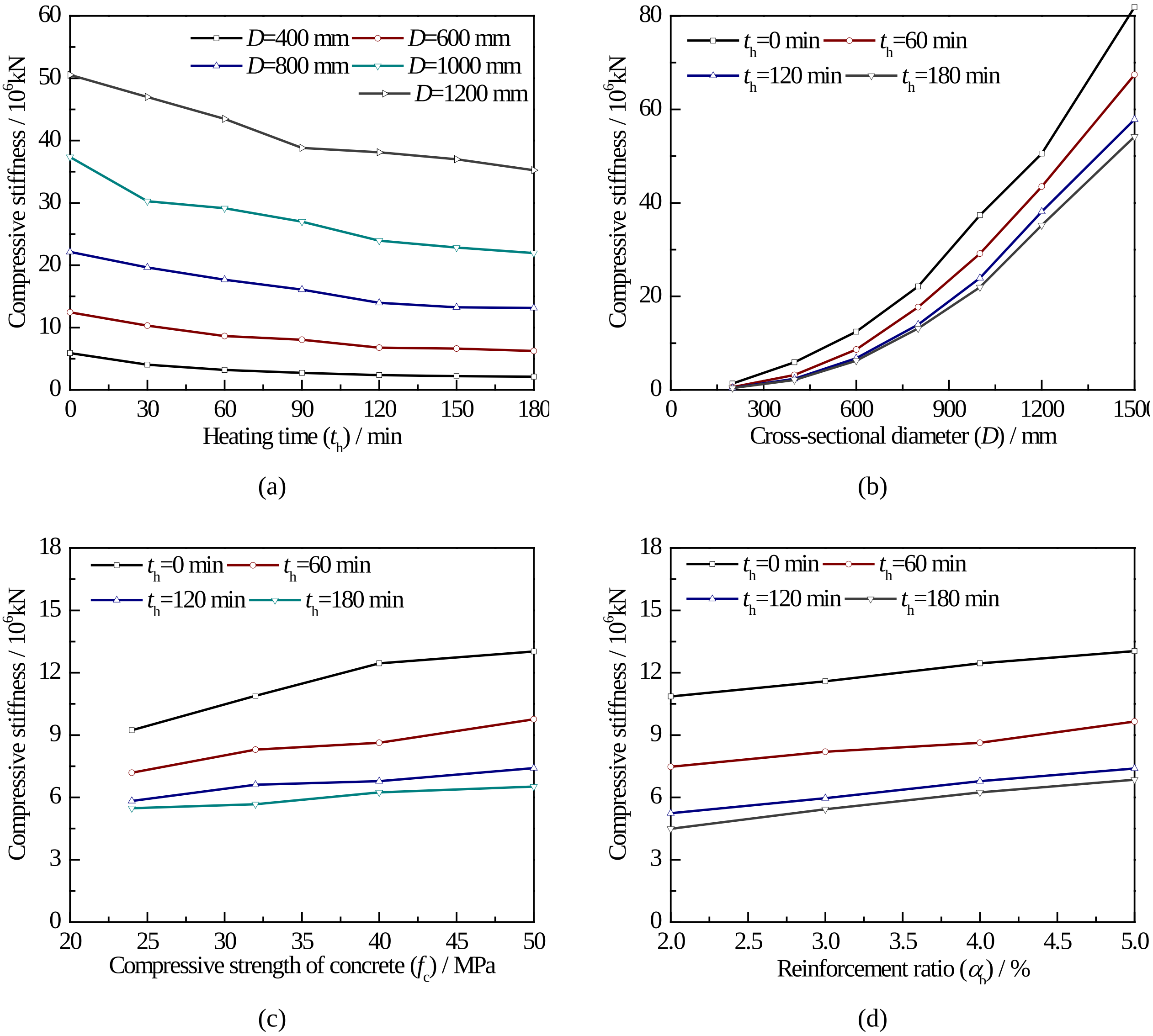

Fig.17 Influences of parameters on compressive stiffness: (a) heating time; (b) cross-sectional dimension; (c) compressive strength of concrete; and (d) reinforcement ratio.

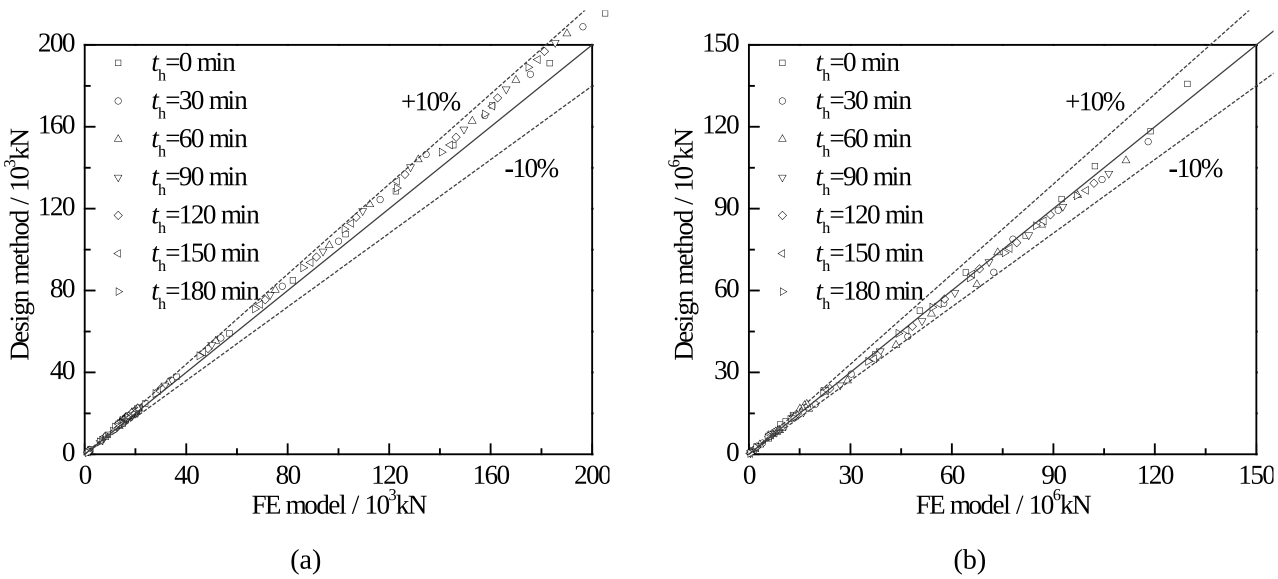

Fig.18 Comparisons of predicted residual capacity and compressive stiffness between the design method and FE model: (a) residual capacity; and (b) compressive stiffness.

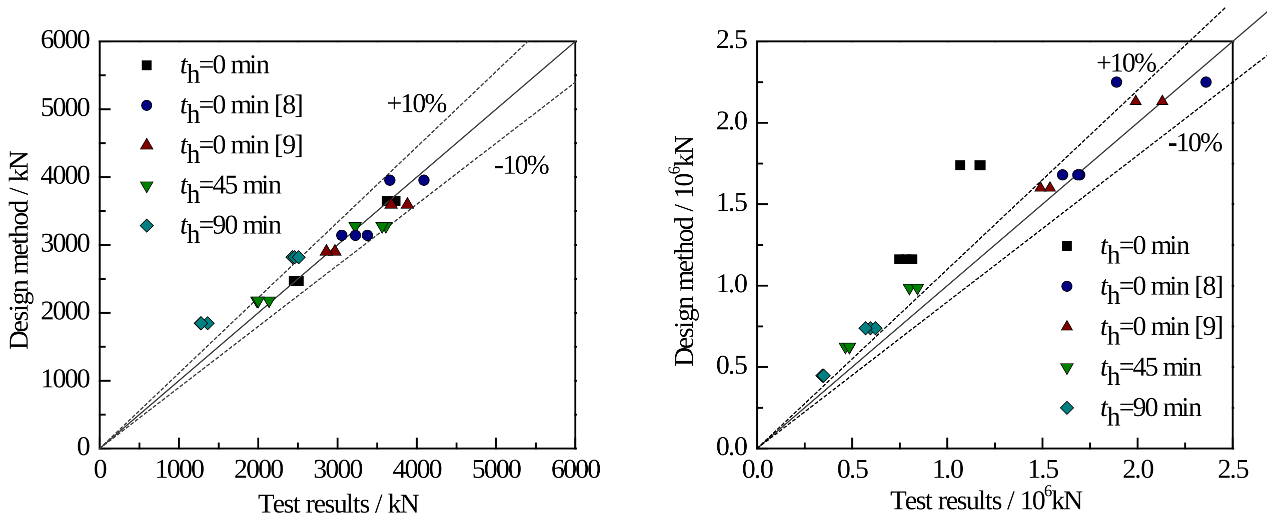

(a)

(b)

Fig.19 Comparisons between predicted and tested results of specimens: (a) residual capacity; and (b) compressive stiffness.

Table 1 Details of test specimens

Column no.	B (mm)			t_s (mm)		α_s (%)	L (mm)	Reinforcing bars	α_b (%)	t_h (min)
	Nominal	Measured		Nominal	Measured					
S200-0-a	200	202	198	1.80	1.76	3.70	600	8B16	4.17	0
S200-0-b	200	200	197	1.80	1.74	3.70	600	8B16	4.17	0
S200-0-c	200	201	198	1.80	1.75	3.70	600	8B16	4.17	0
S200-45-a	200	201	197	1.80	1.75	3.70	600	8B16	4.17	45
S200-45-b	200	200	198	1.80	1.75	3.70	600	8B16	4.17	45
S200-45-c	200	201	196.5	1.80	1.74	3.70	600	8B16	4.17	45
S200-90-a	200	200	197.5	1.80	1.75	3.70	600	8B16	4.17	90
S200-90-b	200	201	198	1.80	1.73	3.70	600	8B16	4.17	90
S200-90-c	200	201	197.5	1.80	1.80	3.70	600	8B16	4.17	90
S250-0-a	250	251	248	2.20	2.22	3.62	750	8B20	4.17	0
S250-0-b	250	251	249	2.20	2.22	3.62	750	8B20	4.17	0
S250-0-c	250	251	247	2.20	2.22	3.62	750	8B20	4.17	0
S250-45-a	250	251	249	2.20	2.23	3.62	750	8B20	4.17	45
S250-45-b	250	251	249	2.20	2.21	3.62	750	8B20	4.17	45
S250-45-c	250	251	249	2.20	2.23	3.62	750	8B20	4.17	45
S250-90-a	250	252	248	2.20	2.22	3.62	750	8B20	4.17	90
S250-90-b	250	251	249	2.20	2.22	3.62	750	8B20	4.17	90
S250-90-c	250	250	249	2.20	2.22	3.62	750	8B20	4.17	90

Table 2 Ambient temperature properties of steel tube after fire exposure times of 0, 45 and 90 minutes

Nominal t_s (mm)	Measured t_s (mm)	t_h (min)	E_s (N/mm^2)	f_y (N/mm^2)	f_{su} (N/mm^2)	ν_s	ε_{sf} (%)
1.80	1.72	0	2.30×10^5	302.8	426.9	0.258	27.9
		45	1.75×10^5	233.0	364.5	0.271	39.2
		90	1.73×10^5	228.5	342.7	0.236	43.5
2.20	2.22	0	2.27×10^5	352.8	523.2	0.271	30.9
		45	1.79×10^5	314.6	463.2	0.239	35.7
		90	1.64×10^5	218.0	403.1	0.247	44.9

Table 3 Properties of longitudinal reinforcing bars

Steel type	Measured d_b (mm)	E_b (N/mm^2)	f_b (N/mm^2)	f_{bu} (N/mm^2)	ε_{bf} (%)
Hot-rolled ribbed	16.37	2.09×10^5	513.5	692.7	26.10
Hot-rolled ribbed	19.56	1.79×10^5	428.3	555.9	21.97

Table 4 Concrete cube strength and elastic modulus

Nominal f_{cu} (N/mm^2)	$f_{cu,28}$ (N/mm^2)	$f_{cu,test}$ (N/mm^2)	$E_{c,test}$ (N/mm^2)	v_c
30	36.79	45.6	21940	0.190

Table 5 Experimental results of the specimens

Group no.	Column no.	EA (10^6kN)	N_y (kN)	$\triangle_y$ (mm)	N_u (kN)	$\triangle_u$ (mm)	$\triangle_{0.85}$ (mm)	$\mu_\triangle$
S200	S200-0-a	0.817	2246.82	2.07	2466.86	2.58	4.27	2.06
	S200-0-b	0.747	2245.06	2.11	2447.94	2.80	4.67	2.21
	S200-0-c	0.785	2274.81	2.08	2511.00	2.86	4.58	2.20
	Averaged	0.783	2255.56	2.09	2475.27	2.75	4.51	2.16
	S200-45-a	0.464	1797.11	2.88	1984.43	4.37	8.94	3.10
	S200-45-b	0.486	1920.46	3.08	2136.02	4.11	6.51	2.11
	S200-45-c	0.485	1800.20	2.75	1999.48	3.85	5.60	2.04
	Averaged	0.478	1839.26	2.90	2039.98	4.11	7.02	2.42
	S200-90-a	0.347	1211.24	2.75	1360.44	4.71	8.30	3.02
	S200-90-b	0.343	1154.96	2.70	1273.86	4.50	6.78	2.51
	S200-90-c	0.350	1134.38	2.51	1280.30	4.48	7.37	2.94
	Averaged	0.347	1166.86	2.65	1304.87	4.56	7.48	2.82
S250	S250-0-a	1.169	3461.27	2.70	3622.67	3.72	-	-
	S250-0-b	1.176	3514.22	2.66	3733.73	3.33	-	-
	S250-0-c	1.068	3541.88	2.87	3715.50	3.51	5.03	1.75
	Averaged	1.138	3505.79	2.74	3690.63	3.52	5.03	1.75
	S250-45-a	0.801	3470.38	3.56	3609.64	4.24	6.31	1.77
	S250-45-b	0.843	2948.47	3.14	3223.79	4.35	6.02	1.92
	S250-45-c	0.875	3351.54	3.26	3561.99	4.19	5.88	1.80
	Averaged	0.840	3256.80	3.32	3465.14	4.26	6.07	1.83
	S250-90-a	0.596	2200.72	3.52	2432.47	5.22	7.15	2.03
	S250-90-b	0.622	2204.60	3.54	2458.58	5.58	9.72	2.75
	S250-90-c	0.570	2307.84	3.83	2510.46	5.31	7.38	1.93
	Averaged	0.596	2237.72	3.63	2467.17	5.37	8.08	2.24

Table 6 Comparisons between average measured maximum temperatures and predicted temperatures

Column no.	Location	Averaged $T_{max,test}$ (^oC)	$T_{max,FE}$ (^oC)	$T_{max,FE}$ / $T_{max,test}$
S200-45min	Steel tube (1, 5, 6, 10)	757	808	1.07
	Bars (11, 12)	392	407	1.04
	Bars (13, 14)	456	491	1.08
	Concrete *d*=30mm (2, 7)	382	412	1.08
	Concrete *d*=50mm (4, 9)	342	393	1.15
	Concrete *d*=100mm (3, 8)	338	386	1.14
S200-90min	Steel tube (1, 5, 6, 10)	947	957	1.01
	Bars (11, 12)	576	589	1.02
	Bars (13, 14)	764	653	0.85
	Concrete *d*=30mm (2, 7)	615	595	0.97
	Concrete *d*=50mm (4, 9)	570	572	1.00
	Concrete *d*=100mm (3, 8)	554	564	1.02
S250-45min	Steel tube (1, 5, 6, 10)	777	804	1.03
	Bars (11, 12)	293	352	1.20
	Bars (13, 14)	444	468	1.05
	Concrete *d*=30mm (2, 7)	321	363	1.13
	Concrete *d*=60mm (4, 9)	262	318	1.21
	Concrete *d*=125mm (3, 8)	243	312	1.28
S250-90min	Steel tube (1, 5, 6, 10)	957	950	0.99
	Bars (11, 12)	499	526	1.05
	Bars (13, 14)	634	630	0.99
	Concrete *d*=30mm (2, 7)	548	548	1.00
	Concrete *d*=60mm (4, 9)	450	487	1.08
	Concrete *d*=125mm (3, 8)	436	481	1.10
		Mean		1.064
		Standard deviation		0.091